Cite as: C. Zhao *et al.*, *Science* 10.1126/science.aal3485 (2017).

Stromal *Gli2* activity coordinates a niche signaling program for mammary epithelial stem cells

Chen Zhao,[1,2*†] Shang Cai,[1*] Kunyoo Shin,[1,2,6] Agnes Lim,[1,3] Tomer Kalisky,[4] Wan-Jin Lu,[1,2] Michael F. Clarke,[1] Philip A. Beachy[1,2,3,5‡]

[1]Institute for Stem Cell Biology and Regenerative Medicine, Stanford University School of Medicine, Stanford, CA 94305, USA. [2]Department of Biochemistry, Stanford University School of Medicine, Stanford, CA 94305, USA. [3]Department of Developmental Biology, Stanford University School of Medicine, Stanford, CA 94305, USA. [4] Faculty of Engineering and Institute for Nanotechnology and Advanced Materials, Bar-Ilan University, Ramat Gan 52900, Israel. [5]Howard Hughes Medical Institute, Stanford University School of Medicine, Stanford, CA 94305, USA. [6]Department of Life Sciences, Pohang University of Science and Technology, Pohang, Gyumgbuk 37673, South Korea.

*These authors contributed equally to this work.

†Present address: Department of Genetics and Genomic Sciences, Icahn School of Medicine at Mount Sinai, New York, NY, USA.

‡Corresponding author. Email: pbeachy@stanford.edu

The stem cell niche is a complex local signaling microenvironment that sustains stem cell activity in organ maintenance and regeneration. The mammary gland niche must support its associated stem cells while also responding to systemic hormonal regulation that triggers pubertal changes. We find that *Gli2*, the major Hedgehog pathway transcriptional effector, acts within mouse mammary stromal cells to direct a hormone-responsive niche signaling program by activating expression of factors that regulate epithelial stem cells as well as receptors for the mammatrophic hormones estrogen and growth hormone. Whereas prior studies implicate stem cell defects in human disease, this work shows that niche dysfunction may also cause disease, with possible relevance for human disorders and in particular the breast growth pathogenesis associated with combined pituitary hormone deficiency (CPHD).

The Hedgehog (Hh) signaling pathway regulates embryonic patterning and postnatal homeostasis of multiple tissues (*1–3*), acting via its major transcriptional effector, Gli2. A specific function for *Gli2* in ductal morphogenesis of the mammary gland was suggested by the defects noted in *Gli2*$^{-/-}$ mutant mouse embryonic mammary gland rudiments engrafted into adult hosts (*4*). In addition, breast under-development at puberty is associated with the human disorder CPHD (*5*), a significant subset of which is caused by loss-of-function or trans-dominant mutations of the *GLI2* gene (*6–8*). In contrast, *Gli2* function appears to be dispensable for embryonic specification of mammary gland rudiments, which instead shows a requirement for expression of the Gli3 repressor of Hh pathway targets in underlying somitic mesoderm (*1* (*9–12*)). Adding further complexity to the role of Hh pathway activity, *Gli2* is expressed in the epithelium of embryonic mammary gland rudiments whereas *Gli2* expression in pubertal and virgin adult mice occurs exclusively in stromal cells (*12*).

Periductal *Gli2* expression in developing mammary

To investigate the role of *Gli2* in postnatal mammary gland growth, we examined *Gli2* expression in the developing gland and manipulated its activity through genetic ablation or hyperactivation. *Gli2* expression occurs intermittently in stromal cells along mammary ducts, but is highly enriched at terminal end buds of the pubertal gland (5 wks; Fig. 1A,B) and at terminal structures of the adult female gland (10 wks; Fig. 1E,F). These regions of the pubertal and adult ducts undergo extensive proliferation and have been suggested as sites for mammary epithelial stem cells (*13–18*). *Gli2*-expressing cells in cross-sections of mammary ducts appear restricted to stromal regions in both pubertal (Fig. 1C-D) and adult mammary gland (Fig. 1G-H), as previously reported (*12*), and in adult male mammary gland as well (fig. S1A). This stromal pattern of *Gli2* RNA and protein expression was confirmed by qPCR and Western blot assays of FACS-sorted stromal vs. luminal or basal epithelial cells (Fig. 1I, J; fig. S1B). The close proximity of *Gli2* expression to mammary ducts (Fig. 1A-H) suggests the possibility of an inductive influence from epithelium in mediating stromal *Gli2* expression. Such an inductive effect was confirmed by the absence of β-galactosidase expression in cleared mammary fat pads of *Gli2*$^{nlacZ/+}$;*NSG* mice (Fig. 1K, left panel), and appearance of stromal β-galactosidase expression upon transplantation of cleared fat pads with FACS-isolated mammary epithelial cells (Fig. 1K, right panel, blue arrowheads; see Methods). We found that TGFβ1, expressed in mammary epithelial cells (*19*), markedly induced expression of *Gli2* in FACS-isolated stromal cells in vitro in a dose-dependent manner (4.5-fold and 8-fold at 5 and 50 ng/ml, respectively; Fig. 1L). The dependence of *Gli2* expression on

TGFβ1 signaling was confirmed in vivo by a 2.2-fold reduction of mammary gland stromal *Gli2* mRNA upon treatment of mice with the TGFβR inhibitor, LY2109761 (Fig. 1M). We note that response to TGFβ does not include expression of *Gli2* in the mammary epithelium; this and other differences in epithelial vs. stromal responses may help account for the complexity of TGFβ effects on mammary development and in carcinogenesis (*19*).

Stromal *Gli2* in pubertal mammary development

In order to genetically ablate *Gli2* function in stromal cells by site-specific recombination, we examined the extent of coincident expression of β-galactosidase from the $Gli2^{nLacZ}$ reporter with Cre recombinase from the $Fsp1^{Cre}$ allele. In mice of the genotype $Fsp1^{Cre}$;$Rosa26^{mTmG/+}$;$Gli2^{nLacZ}$, Cre recombinase causes a switch of expression of the membrane-associated red fluorescent protein mT to expression of the membrane-associated green fluorescent protein mG (fig. S1C). In these mice *Gli2* mRNA, indicated by expression of β-galactosidase, is enriched in mG-expressing cells (fig. S1D), and a quantitative comparison revealed that most cells expressing β-galactosidase from the $Gli2^{nlacZ}$ allele also expressed mG (73 ± 12%; Fig. 2A, B). The $Fsp1^{Cre}$ driver thus appears suitable for Cre-mediated ablation of a *floxed* conditional allele of *Gli2* ($Gli2^{fl}$) in stromal cells of the mammary gland, which is the exclusive site of *Gli2* expression in mammary glands of pubertal and virgin adult females. $Fsp1^{Cre}$ combined with $Gli2^{fl/fl}$ or $Gli2^{fl/nlacZ}$, hereafter referred to as $Gli2^{\Delta S}$ (genetic ablation of *Gli2* is characterized in fig. S2A) produced a significant delay of mammary gland development at pubertal stages (5 weeks; fig. S2B). By adult stages, $Gli2^{\Delta S}$ mice gradually developed a hypoplastic mammary gland with greatly enlarged ducts and severely disrupted terminal end structures (6-10 weeks; Fig. 2C and fig. S3). Histological examination and FACS analysis further revealed reduced levels of type I, type II and type IV collagen fibers and a five-fold reduction in periductal stromal cells (2.3% vs. 10.9%; Fig. 2E and fig. S2C). The combined ductal and stromal abnormality, as measured by the ratio of ductal diameter to stromal thickness (ductal:stromal ratio or DSR), was highly significant in $Gli2^{\Delta S}$ mice (Fig. 2D).

To examine the effect of increased Gli2 activity, $Fsp1^{Cre}$ was used to drive stromal expression of Smo^{M2}, which encodes a constitutively activating form of the seven-transmembrane Smo component of the Hedgehog pathway (*20*, *21*), in mice of the genotype $Fsp1^{Cre}$;$R26^{SmoM2}$. These mice had a maximum lifespan of 12 weeks (fig. S4A), but in marked contrast to $Gli2^{\Delta S}$ displayed a dramatic expansion of the mammary gland stromal compartment, as indicated by increased collagen expression and a 20-fold increase in the percent of stromal cells expressing the proliferative marker, Ki67 (1.2 ± 0.5 vs. 23 ± 4; fig. S4B-D). Both the stromal expansion and proliferative effects of stromal Smo^{M2} expression were reversed by additional ablation of *Gli2*, which functions downstream of *Smo*, in mice of the genotype $Fsp1^{Cre}$;$R26^{SmoM2}$;$Gli2^{fl/fl}$. This reversal demonstrates that Smo^{M2} effects are dependent on *Gli2*. The contrasting effects of *Gli2* genetic ablation or hyper-activation indicate that the overall abundance of stromal elements within stromal cells is dictated by the presence and activity of Gli2.

Stromal *Gli2* supports mammary stem cell activity

The developmental delay and terminal defects in mammary ducts of $Gli2^{\Delta S}$ mice suggested that ductal epithelial cell proliferation might be impaired. We indeed noted a qualitative decrease in epithelial staining for the Ki67 indicator of proliferative activity in adult mammary gland sections from $Gli2^{\Delta S}$ mice (fig. S5A), and further found by quantitative FACS-based analysis a 2.6-fold reduction of epithelial cells labeled by incorporation of the nucleoside analog EdU in $Gli2^{\Delta S}$ as compared to $Gli2^{WT}$ mice (1.3% vs. 0.5%; Fig. 3A). In contrast, markers indicative of epithelial differentiation were not significantly different in their expression in immunofluorescence staining (fig. S5A) and the relative proportions of FACS-isolated luminal vs basal populations in $Gli2^{\Delta S}$ mice were not notably different from $Gli2^{WT}$ mice (right panel in fig. S5A). To further investigate reduced levels of proliferation, we cultured mammary epithelial cells from $Gli2^{\Delta S}$ and $Gli2^{WT}$ mice ex vivo in a Matrigel-based colony-forming assay. We found that primary epithelial cells from $Gli2^{WT}$ mice formed 3 times more colonies than cells from $Gli2^{\Delta S}$ mice (Fig. 3B). Collectively, these data indicate that removal of *Gli2* in $Fsp1^{Cre/+}$ stromal cells leads to a defect in the proliferation of the mammary epithelium.

The growth and regeneration of mammary epithelium depends on the activity of mammary epithelial stem cells (MaSCs), functionally characterized by measurement of mammary repopulating units (MRU) upon transplantation of FACS-isolated cells into cleared mammary fat pads (*22*, *23*). The activity of MaSCs depends critically upon signals provided by the mammary stroma (*24*). As MaSCs are enriched in myoepithelium (*22*, *23*), the basal layer of the mammary epithelium that directly contacts the stromal environment, we sought to investigate how stromal loss of *Gli2* may affect the epithelial stem cell niche. To this end we first compared MaSCs from $Gli2^{WT}$ or $Gli2^{\Delta S}$ mice in a competitive mammary gland repopulation assay by FACS isolation of cells from the upper portion (~50%) of the basal epithelial cell population (Lin^-, $CD24^+$, $CD49f^{high}$; Fig. 1I) of $Gli2^{\Delta S}$ or littermate $Gli2^{WT}$ mice; these upper basal epithelial cells, enriched in MaSCs (*22*, *23*), are fluorescent red as mT expression is not affected by the stromal $Fsp1^{Cre}$ driver. These red fluorescent cells, were mixed with similarly FACS-isolated green fluorescent cells (expressing EGFP) from con-

trol mice, and the mixtures were injected into the left and right cleared fat pads, respectively, of recipient NSG animals (Fig. 3C). Within 9 weeks of transplantation the red fluorescent cells from *Gli2*^{WT} mice contributed equally with green fluorescent control cells to the regenerated ductal tree (44%:56%), whereas red fluorescent cells from the *Gli2*$^{\Delta S}$ mice contributed minimally (7%:93%) (Fig. 3C, D and fig. S5B). Cross-sections of mammary ducts from these transplanted animals showed no notable differences in periductal stromal cells and no ductal enlargement in the outgrowths derived from epithelial cells of *Gli2*^{WT} or *Gli2*$^{\Delta S}$ mice (Fig. 3C). MaSCs derived from the upper basal epithelial population from *Gli2*$^{\Delta S}$ mice thus are defective in their regenerative activity, with reduced colony-forming potential in vitro (Fig. 3B) and a dramatically impaired ductal outgrowth potential in vivo in competitive transplantation experiments (Fig. 3C).

To further examine the effect of stromal *Gli2* function on MaSCs, we measured MRUs of FACS-isolated upper basal epithelial cells from GFP-expressing mice upon transplantation into cleared mammary fat pads of *Gli2*$^{\Delta S}$ or *Gli2*^{WT} littermate mice (Fig. 3E). We found that transplantation into control host animals with at least one *Gli2*^{WT} allele in their mammary stroma generates ductal outgrowths five-fold more efficiently as compared to *Gli2*$^{\Delta S}$ hosts (outgrowth efficiencies: 1/618 vs. 1/2920; Fig. 3F). Interestingly, ductal outgrowth in *Gli2*$^{\Delta S}$ mice was limited to a small area (<20 mm^2), and these outgrowths were often malformed with enlarged mammary ducts and a thin layer of stromal cells (Fig. 3E and fig. S5C) with reduced *Gli2* expression (fig. S5D). Importantly, the difference in MaSC functional activity measured in these transplantation assays is solely a function of the *Gli2* status of the host stromal environment, as the donor cells are from mice that are wild-type except for expression of GFP. These findings thus suggest that the Gli2 activity in FSP+ cells controls a niche-signaling program that regulates mammary stem cell activity, and that this program is disrupted in *Gli2*$^{\Delta S}$ mice.

Locally acting factors mediate stromal *Gli2* activity

In addition to input from local stromal cells, mammary morphogenesis and the MaSC pool are also regulated by other factors including the systemic hormonal environment (*25*) as well as immune cell surveillance (*26*). We therefore investigated the possibility that *Gli2* activity in other cells or organs affects mammary development. To this end, we first analyzed co-expression of *Fsp* and *Gli2* in ovary, the major organ for female hormone production (e.g., estrogen, progesterone). We observed few double positive cells in corpus luteum (0.16%, n=1927), and no co-expression in follicles (0%, n=2418) (Fig. 4A-D), suggesting that *Gli2* ablation is a rare event in the ovaries of our *Gli2*$^{\Delta S}$ mice. In addition, and consistent with the lack of *Fsp1* and *Gli2* co-expression in ovary, *Gli2*^{WT} and *Gli2*$^{\Delta S}$ mice had statistically indistinguishable estrogen levels (Fig. 4E, p=0.5) that were comparable to those previously reported (*27*). We similarly noted little co-expression of *Fsp1* and *Gli2* in the pituitary, and no significant change in serum growth hormone (GH) or prolactin levels (Fig. 4F-H). These data collectively suggest that the *Gli2*$^{\Delta S}$ mice maintain a hormonal environment similar to that of *Gli2*^{WT} littermates during development.

We next investigated potential co-expression of *Fsp1* and *Gli2* in mammary macrophages, which are reported to play a role in mammary development during puberty (*26*). Although we did observe *Gli2* expression in a minuscule fraction (~1%) of mammary cells expressing the macrophage marker F4/80 (Fig. 5A, n=1247), we detected no *Fsp1* expression in F4/80+ cells (Fig. 5B, n=1248), indicating that *Fsp1*^{Cre}-driven ablation of *Gli2* in mammary macrophages is highly unlikely. To further exclude a possible defect in mammary macrophages in the *Gli2*$^{\Delta S}$ phenotype, we transplanted wild-type stromal cells and macrophages into the mammary fat pads of pubertal *Gli2*$^{\Delta S}$;NSG recipient mice (Fig. 5C). We noted that although stromal cells successfully rescued ductal enlargement with restoration of periductal collagen and extracellular matrix (Fig. 5C-F, n=3), macrophage transplantation did not provide any rescuing activity. These results suggest that macrophages contribute little if anything to the epithelial activity lost in *Gli2*$^{\Delta S}$ mice. The sufficiency of locally implanted stromal cells to rescue the *Gli2*$^{\Delta S}$ mammary phenotype furthermore excludes a role for loss of systemic factors such as pituitary or ovarian mammatropic hormones in the *Gli2*$^{\Delta S}$ mammary phenotype.

To identify stromal factors induced by *Gli2* activity, we compared gene expression of FACS-isolated *Fsp1*^{Cre}-marked stromal cells from *Gli2*$^{\Delta S}$ or *Gli2*^{WT} littermates by microarray analysis), and identified genes encoding paracrine factors such as *Igf1*, *Wnt2*, *Hgf*, *Fgf7*, and *Bmp7*; we also identified down-regulated genes encoding estrogen receptor (*Esr1*), growth hormone receptor (*Ghr*), and other genes typically expressed in stromal cells. Of particular interest among the paracrine factors, WNT signals sustain the activity of MaSCs in vivo and in ex vivo culture (*28*, *29*), and functional inactivation of *Igf1* or its epithelially expressed receptor, *Igf-1r*, both lead to development of hypoplastic mammary glands with terminal end bud abnormalities (*30*, *31*), similar to the defects we observe in *Gli2*$^{\Delta S}$ mice. The down-regulation of these genes was confirmed by qRT-PCR of bulk stromal cells from *Gli2*^{WT} and *Gli2*$^{\Delta S}$ mice (Fig. 6A), and was further quantified by qRT-PCR from single cells (fig. S6A; summarized in Fig. 6B). *Igf1* and *Wnt2* were expressed in 7% and 9% of individual *Gli2*^{WT} stromal cells, respectively, but in 0% of *Gli2*$^{\Delta S}$ stromal cells (Fig. 6B). Our single cell analysis was validated by the expression of *Gli2* in 19% of *Fsp1*^{Cre}-marked *Gli2*^{WT} stromal cells (Fig. 6B), consistent with our immuno-

fluorescence analyses (Fig. 2A,B). Interestingly, the *Gli2*^{nlacZ} reporter is expressed within the thin stromal layer that remains in *Gli2*$^{\Delta S}$ mice in a pattern similar to that of *Gli2*^{nlacZ} within control mice (Fig. 6C), indicating that these cells may be correctly specified but fail to function normally, due to loss of Gli2 protein activity. These results collectively show that the Gli2 transcription factor is critical for expression of mammary stem cell niche signals.

Mammatrophic hormone response requires stromal *Gli2*

Previous studies have shown that MaSCs respond to the mammatrophic hormones estrogen and growth hormone (*32*, *33*). MaSCs do not, however, express the receptors for these hormones (*34*), indicating that the mammatrophic hormone effect is indirect. Mammary stroma is a major mediator of hormone effects on MaSC activity (*24*) and we find that expression of estrogen receptor and growth hormone receptor are dramatically reduced from 7% and 14%, respectively, to 2% of individual stromal cells in *Gli2*$^{\Delta S}$ mice (Fig. 6B). We therefore examined the *Gli2*-dependence of hormone response in FACS-isolated *Fsp1*^{Cre}-marked mammary stromal cells, and indeed found that stimulation with growth hormone (GH) or with estrogen revealed significantly impaired induction of their target genes *Igf1* or *Hgf*, respectively, in cells from *Gli2*$^{\Delta S}$ as compared to *Gli2*^{WT} mice (2.88-fold reduction for *Igf1* and 3.16-fold reduction for *Hgf*; Fig. 6D,E), reflecting the significant reduction in expression of receptors for these hormones (fig. S7).

These defects in hormonal response of mammary stroma are reminiscent of the incomplete response of patients suffering from the disorder CPHD (Combined Pituitary Hormone Deficiency) to hormonal supplementation. This supplementation is provided because multiple peptidic pituitary hormones and steroidal hormones induced by pituitary hormones are deficient due to the congenital hypopituitarism associated with CPHD. Supplementation with GH rescues height defects in these patients (*35*, *36*), but abnormal breast development often is not improved, even with estrogen supplementation (*5*). *Gli2*$^{\Delta S}$ mice produce normal levels of pituitary hormones such as GH and prolactin (Fig. 3G-H), as *Gli2* expression in the pituitary is not affected (*Fsp1*^{Cre} and *Gli2*^{nlacZ} expression in the pituitary do not overlap; Fig. 4F). Despite intact pituitary hormone production, however, *Gli2*$^{\Delta S}$ mice nevertheless show abnormal mammary gland development, as described above. *Gli2*$^{\Delta S}$ mice thus do not share the pituitary hormonal deficiencies of CPHD patients but do share the resistance to hormone treatments, which likely contributes to the pathogenesis of mammary abnormalities in CPHD patients. Consistent with this interpretation, we find that *hGLI2*, like m*Gli2*, is expressed predominantly in stromal breast cells (fig. S8).

If, as our findings suggest, stromal *Gli2* mediates hormonal response and the expression of niche signals that support epithelial stem cell activity, it should be possible to rescue mammary defects seen in *Gli2*$^{\Delta S}$ mice by providing missing niche signals from an exogenous source. We therefore tested the effect of slow-release polymer implants containing secreted protein signals in the intact mammary of *Gli2*$^{\Delta S}$ mice, focusing in particular on IGF1 and a canonical WNT family protein because of the well-established roles of these signals in mammary development (*28–31*), and using GH as a control. Ex vivo assays showed that GH, IGF1 and WNT2b proteins embedded in the slow-release polymer, polyethylene-co-vinyl acetate (Elvax40), were gradually released over 2-8 days and were able to stimulate pathway-specific target genes (fig. S9A-G). For in vivo experiments, the effects of control or factor-containing polymer implants surgically placed in the mammary glands of *Gli2*$^{\Delta S}$ mice were assessed after 7 days by whole mount analysis and qPCR (Fig. 7A).

We indeed confirmed, that, although GH-containing Elvax40 implants increased the number of terminal structures 5-fold in *Gli2*^{WT};NSG host mice (5.625 ± 1.21; fig. S9B-C), in *Gli2*$^{\Delta S}$;NSG mice these implants failed to stimulate *Igf1* expression and did not change terminal structure growth at the implantation site (Fig. 7B-D). In contrast to GH, IGF1-containing implants increased terminal structure formation in the vicinity of the implants 7-fold in pubertal (psd40) and 5-fold in adult (psd70) *Gli2*$^{\Delta S}$ mice (Fig. 7E-F, fig. S10A). IGF1 target genes *Egr1* and *M-Csf* also were reliably induced near the site of the implants (Fig. 7G), confirming the efficacy of IGF1 delivery. As compared to IGF1 alone, implants containing both IGF1 and WNT2b showed an even greater effect in inducing a 13-fold increase in terminal structure growth at the adult stage (Fig. 7H,I) in *Gli2*$^{\Delta S}$ mice, and consistently induced the expression of *M-Csf* and *Axin2* (Fig. 7J); *Axin2* expression indicates Wnt response, which promotes the survival and self-renewal ability of mammary epithelia (*29*). Together these results suggest that, although the mammary abnormalities in *Gli2*$^{\Delta S}$ mice fail to respond to growth hormone stimulation, the terminal growth defects of the mammary ductal tree can be rescued in part by local supplementation with the GLI2-dependent paracrine factors IGF1 and WNT2b.

Conclusions

Although the cellular constitution and signaling activity of the stem cell niche is coming into focus in a variety of tissues, the genetic regulatory factors that specify the niche and thus create a favorable environment for stem cell function have not been identified. The activity of such factors is particularly intriguing in organs such as the breast, where the niche provides local signals for tissue homeostasis but

also must be entrained by circulating hormones that induce the dramatic changes of puberty. Here we find with a *Gli2*^{nLacZ} reporter and a stromal-specific Cre driver that *Gli2* is predominantly expressed in periductal stroma of the mammary gland of pubertal and virgin adult mice, and encodes a functionally critical regulator that specifies niche activity in support of mammary epithelial stem cells (Fig. 8). One aspect of this regulatory activity is the induction, direct or indirect, of stem cell support factors, including IGF and WNT signaling proteins. The GLI2 transcription factor thus appears to control the niche signaling program for MaSCs. *Gli2*$^{\Delta S}$ mice lacking stromal *Gli2* function consequently suffer from a severe defect in regenerative activity of epithelial stem cells. A second aspect of *Gli2* activity is the induction of receptors for mammatrophic hormones such as growth hormone and estrogen in stromal cells such that they become competent to respond to circulating hormones, thereby placing niche signaling activity under hormonal control. This hormonal response is also lost in *Gli2*$^{\Delta S}$ mice (Fig. 8). Thus, our analysis provides insight into the mechanism that coordinates systemic mammatrophic hormone action and activity of the local epithelial stem cell niche, namely, that a single transcription factor, GLI2, controls both the expression of hormone receptors and the stromal niche signaling program.

Our findings in *Gli2*$^{\Delta S}$ mice imply that a defective stem cell niche environment may underlie the pathogenesis of breast defects seen in the human disorder, CPHD. Though several degenerative and aging-related diseases have been tentatively ascribed to defects in stem cells themselves, dysfunction of a supporting niche has not previously been linked to human disease (*37*). By indicating that niche failure can cause disease, our study asserts the central role of the niche in controlling stem cell activity and raises the possibility of niche dysfunction in other human diseases. Furthermore, by directly providing *Gli2*-dependent mammary niche signaling factors to rescue aspects of the *Gli2*$^{\Delta S}$ mammary in mice, our work suggests a potential therapeutic intervention for patients with hormone-refractory CPHD.

METHODS

Mice

Female mice at pubertal (5 weeks) or adult (10 weeks) stages were used for all experiments. *Gli2*^{nLacZ} mice (*38*) were first bred with *Gli2*^{flox} mice (*39*), then with *Rosa26*$^{mTmG/+}$ mice (*40*) to generate *Gli2*$^{flox/nLacZ}$ or *Gli2*$^{nLacZ/+}$;*Rosa26*$^{mTmG/+}$ mice. *Fsp1Cre* mice (*41*) were crossed to *Gli2*$^{flox/flox}$ to generate *Fsp1Cre;Gli2*$^{flox/+}$ or with *Rosa26*$^{mTmG/mTmG}$ mice to generate *Fsp1Cre;Rosa26*$^{mTmG/+}$ strain. *Fsp1Cre;Gli2*$^{flox/+}$ mice were then crossed with *Gli2*$^{flox/nLacZ}$ mice to obtain littermate *Gli2*$^{flox/+}$ and *Fsp1Cre;Gli2*$^{flox/nLacZ}$ mice. The *Fsp1Cre;Rosa26*$^{mTmG/+}$ strain was crossed to *Gli2*$^{flox/flox}$ strain to generate Fsp1Cre;*Rosa26*$^{mTmG/+}$;*Gli2*$^{flox/+}$ mice which were subsequently bred to *Gli2*$^{nLacZ/+}$;*Rosa26*$^{mTmG/+}$ to obtain littermate Fsp1Cre;*Rosa26*$^{mTmG/+}$, FspCre1;*Rosa26*$^{mTmG/+}$;*Gli2*$^{nLacZ/+}$ and Fsp1Cre;*Rosa26*$^{mTmG/+}$;*Gli2*$^{nLacZ/flox}$ mice. NSG mice were extensively bred and back-crossed with Fsp1Cre;*Gli2*$^{nLacZ/flox}$ through 6 generations to obtain *Gli2*$^{flox/+}$;*NSG*, *Gli2*$^{nLacZ/+}$;*NSG,* Fsp1Cre;*Gli2*$^{flox/flox}$;NSG, and Fsp1Cre;*Gli2*$^{nLacZ/flox}$;NSG mice. All mouse strains except as otherwise indicated were obtained from Jackson Laboratories. For each experiment, mice of the same genotypes were randomly selected for experiments and investigators were blinded for outcome assessment. All procedures were performed under an assigned protocol (14586) approved by the Administrative Panel on Laboratory Animal Care (APLAC) at Stanford University.

Antibodies and reagents

The following antibodies were purchased: chicken polyclonal anti-β-Gal antibody (Abcam, CAT:ab9361), rabbit polyclonal anti-CK14 antibody (Covance, CAT:PRB-155P), rabbit polyclonal anti-Ki67 antibody (Abcam, CAT: ab15580), Cy3-conjugated mouse monoclonal anti-smooth muscle actin antibody (Sigma, CAT: C6198), rat anti-CK8 antibody (DSHB, TROMA-I), rabbit polyclonal anti-collagen I antibody (Abcam, CAT: ab21286), goat polyclonal anti-NKCC1 antibody (Santa Cruz, CAT:sc-21545) guinea pig anti-Gli2 antibody was obtained from Dr. Eggenschwiler at University of Georgia, APC-conjugated rat anti mouse F4/80 (Biolegend), rabbit polyclonal anti-S100a4 (Biolegend). Dylight 488-labeled goat anti-chicken IgY, Alexa 488-labeled donkey anti rabbit IgG and Alexa 647-labeled donkey anti-goat IgG were purchased from Jackson ImmunoResearch. Alexa 488-labeled goat anti-rabbit IgG, Alexa 594-labeled goat anti-rabbit IgG, and Alexa 647-labeled goat anti-rat IgG were purchased from Invitrogen. Trichrome straining kit (25088-100) was purchased from Polysciences Inc. Rat/mouse growth hormone ELISA kit was purchased from Millipore (EZRMGH-45K). Mouse prolactin ELISA kit was purchased from Abcam (ab100736). Mouse Igf1 ELISA kit was purchased from Raybiotech (ELM-IGF1). Mouse Wnt2B ELISA kit was purchased from MYBioSource (MBS946031). Click-IT®Plus EdU Alexa Fluor®647 flow cytometry assay kit (C10634) was purchased from Invitrogen. Poly Ethylene-co-vinyl acetate (Elvax40) beads (340502) were purchased from Sigma. Recombinant mouse Igf1 (791-MG-050) and recombinant mouse Wnt2b (customized quantity) were purchased from R&D Systems. Mouse growth hormone (CYT-540) was purchased from Prospecbio. 48.48 Dynamic Array Chips (BMK-M.48.48) for single cell analysis were purchased from Fluidigm. Ortho-nitrophenyl-β-galactoside (ONPG) was purchased from Thermo-Scientific (CAT:34055). TGFβRI/II in-

hibitor, LY2109761, was purchased from XCESSBIO in a customized quantity.

Mammary cell preparation and flow cytometry

Mammary glands from adult mice (10-week-old) were dissected and minced. Single cell suspensions were made by digestion of minced tissue with culture medium (DMEM/F12, 5% fetal bovine serum, 1% penicillin-stretomycin-glutamine) containing collagenase/hyaluronidase cocktail solution (StemCell Technologies, 07912) for 3 hours at 37°C, followed by sequential 5 min treatments with red blood cell lysing buffer (Sigma, R7767), 0.25% Trypsin-EDTA and 0.1mg/ml DNase in 0.1U/ml dispase with gentle pipetting. Cell suspension was then filtered through 40 μm cell strainers and applied to subsequent FACS isolation. PE/Cy7 conjugated anti-mouse CD24 (Rat, clone M1/69), APC conjugated anti-mouse CD49f (Rat, clone GoH3), PerCP/Cy5.5 conjugated anti-mouse CD31 (Rat, clone 390), PerCP/Cy5.5 conjugated anti-mouse CD45 (Rat, clone 30-F11), and PerCP/Cys5.5 conjugated anti-mouseTer119 (Rat, TER-119) were purchased from BioLegend. Antibodies were then incubated with strainer filtered mammary cells in HBSS with 2% FBS for 20 min on ice. All FACS analysis and cell sortings were performed using FACS aria II (Becton Dickinson).

EdU flow cytometry

In vivo EdU labeling was accomplished by intraperitoneal injection of EdU (150ug per 10 g of body weight). Mammary glands were collected after 3 hours and prepared as single cell suspensions, followed by click-it chemistry for EdU staining and surface markers-based staining (CD24-PE/Cy7, CD49f-APC, CD31-PerCP/Cy5.5, CD45-PerCP/Cy5.5, Ter119-PerCP/Cy5.5) to separate stromal, luminal and basal populations. EdU staining cells in stromal negative population were then presented as percent to parental cells.

Liquid β-galactosidase assay

FACS-isolated mammary stromal cells were cultured *ex-vivo* and treated with indicated concentrations of TGFβ with or without TGFβRI/II inhibitor, LY2109761. Cells were lysed and incubated with colorimetric β-gal substrate, ortho-Nitrophenyl-β-galactoside (ONPG). β-gal activity as indicated by OD_{420} was measured at indicated conditions.

In vitro colony formation assay

To compare ex vivo colony forming activity (CFA) of mammary epithelial cells derived from different backgrounds, we adopted an established 3D On-Top assay (*42*). Briefly, Matrigel (BD Bioscience) was thawed and applied to the bottom of 24-well plate at a volume of 120ul per well, followed by polymerization at 37°C for 15 min. FACS-isolated mammary epithelial cells were resuspended in stock buffer (DMEM/F12, 10% FBS) at a density of $2X10^5$ cells per ml, serial diluted in Matrigel containing buffer (DMEM/F12, 10%FBS, 50% Matrigel) and plated on top of the polymerized Matrigel. Culture medium was changed every 48 hours. Primary colony numbers were scored after 14 days in culture, followed by sequential PBS-EDTA treatment and extraction of 3D-cultured mammary colonies into single cell suspensions.

Histology analysis

Gli2^{WT} and *Gli2*$^{\Delta S}$ mice were euthanized at the indicated ages. The 2nd/3rd and/or the 4th mammary glands were dissected. For whole mount carmine alum analysis, mammary glands were fixed in Carnoy's fixative for 3 hours, followed by serial rehydration, carmine alum staining and serial dehydration. Mammary glands were then cleared with xylenes and mounted with permount. For whole mount X-Gal analysis, mammary glands were fixed in X-Gal fixative (2% paraformaldehyde, 0.2% glutaraldehyde) for 30 min at ambient temperature, followed by serial rehydration, overnight carmine alum staining, dehydration and clearance with xylenes. For X-Gal staining, H&E staining, and trichrome staining, mammary glands were fixed and cut as paraffin sections for H&E or trichrome staining or as cryosections for X-Gal staining. X-Gal, H&E, and trichrome staining on mammary sections was performed as described previously (*43*).

Immunofluorescence and confocal microscopy

Dissected mammary glands were fixed in 4% paraformaldehyde, serially dehydrated, and processed as four micrometer paraffin sections. Paraffin sections were cleared with xylenes, rehydrated and subjected to antigen-retrieval in citric acid-based buffer by the pressure cooker method (*44*). For immunostaining, tissue sections were rinsed in PBS, then blocked in blocking solution containing 3%BSA, 0.25% Triton X100 and serum of the host species used to generate the secondary antibody (10% goat serum or 10% donkey serum). An hour after blocking, diluted primary antibodies in blocking buffer were then incubated with sections overnight at 4°C in a humidified chamber. Sections were then washed three times with PBS containing 0.25% Triton X-100 and incubated with appropriate secondary antibodies diluted 1:1000 in blocking solution for 1 hour at ambient temperature, followed by three washes and mounting with Prolong Gold mounting reagent with DAPI (Invitrogen). Immunofluorescence images were obtained using a Zeiss LSM 510 inverted confocal microscope, processed for publication with Zeiss LSM5 Image Browser software and are representative images from one of three experiments.

Mammary fat pad transplantation

FACS-isolated cells were re-suspended in a cocktail buffer with 50% DMEM/F12 (20%FBS), 50% Matrigel, and 0.04%Trypan Blue (Sigma). Cells were injected into cleared mammary gland fat pads of 3-week-old female mice. Repopulated mammary glands were harvested 9 weeks post-transplantation. Outgrowths of repopulated mammary ductal structures were imaged under a fluorescence dissection microscope (Leica). For macrophage and stromal cell rescue assay, macrophages (identified by F4/80) and Fsp+ stromal cells (identified by GFP) from the mammary glands of Fsp-cre *Gli2*$^{lacz/wt}$ mTmG mice were injected into the inguinal fat pads of 3 week-old *Gli2*$^{\Delta S}$ NSG recipient mice at 10k cells/gland with 50% of matrigel+DMEM F12 medium. Two months after the injection, mammary glands were dissected and analyzed by whole mount and IHC.

Mammary in vivo competitive repopulation assay

Green color labeled Lin$^-$CD24$^+$CD49f^{high}GFP$^+$ basal cells isolated from *Gli2*^{WT} mice were mixed in equal number with red color labeled Lin$^-$CD24$^+$CD49f^{hi}GFP$^+$ basal cells isolated from *Gli2*^{WT} mice (Green *Gli2*^{WT}: Red *Gli2*^{WT}) or from *Gli2*$^{\Delta S}$ (Green *Gli2*^{WT}: Red *Gli2* $^{\Delta S}$) mice. These mixes were transplanted bilaterally into cleared mammary gland fat pads of immune-deficient NOD-SCID IL2rγnull (NSG) mice. Outgrowths in this competitive mammary repopulation assay were examined 9 weeks after transplantation.

Mammary regeneration assay

Lin$^-$CD24$^+$CD49f^{hi}GFP$^+$ basal cells derived from EGFP$^+$ mice were serially diluted as indicated and transplanted into cleared mammary gland fat pads of *Gli2*^{WT};NSG mice with at least one functional allele of *Gli2* (*Gli2*$^{flox/+}$;NSG or *Gli2*$^{nLacZ/+}$;NSG) or into *Gli2*$^{\Delta S}$;NSG littermates (*Fsp1Cre;Gli2*$^{flox/nLacZ}$*;NSG* or *Fsp1Cre;Gli2*$^{flox/flox}$*;NSG*). Mammary outgrowth frequency and size of outgrowths were measured. Outgrowth frequency (repopulation frequency) was calculated by L-Calc™ software of StemCell Technologies. Due to limited numbers of matching *Gli2*^{WT};*NSG* and *Gli2* $^{\Delta S}$;NSG within a single litter, data presented in the table summarize transplantation results in mice from several different litters.

RNA extraction and microarray analysis

Total RNAs of FACS-isolated stromal population from *Gli2*^{WT} and *Gli2*$^{\Delta S}$ mice were extracted by Trizol and RNeasy Plus min kit (Qiagen). Concentration and quality of extracted RNAs were determined by Agilent 2100 Bioanalyzer (Agilent Technologies). RNA samples were hybridized to the Mouse Gene 2.0 ST microarray chips and scanned in accordance with manufacturer's protocol (data available at https://www.ncbi.nlm.nih.gov/geo/query/acc.cgi?acc=GSE66820). Expression values normalized and differentially expressed genes were identified using Transcriptome Analysis Console (TAC). Genes showing a fold change of 1.5 (log2) were highlighted in functional annotation analyses. Expression changes of genes of interests by microarray analysis were validated via quantitative rtPCR analysis.

Single cell FACS isolation and data analysis

GFP labeled mammary stromal cells of *Gli2*^{WT} and *Gli2*$^{\Delta S}$ mice were FACS-isolated (5000 cells per genotype), followed by single cell FACS isolation into 96-well plates. Sorted single cells on a 96-plate format were lysed by hypotonic pressure, and mRNA expression levels (threshold cycles, Ct) of 48 genes in 48 cells were measured by microfluidic single cell RT-qPCR reaction in two 48X48 format Fluidigm chips (*45*, *46*) (Fluidigm, CA). Data analysis was performed with Matlab (Mathworks, MA).

Slow-release polymer implantation assay

GH, IGF1, and IGF1/WNT2Bwere prepared as slow-release proteins in Elvax40-based polymers (*47–49*). Briefly,lyophilized BSA (20 mg) alone or in a mixture with the indicated amount of GH, IGF1 or IGF1/WNT2B were dispersed in 0.125 ml of Elvax40 that had been dissolved in dichloromethane [20% wt/vol] The mixture was quick-frozen and dried in a rotary evaporator, then the polymer matrix with entrapped proteins was cut to size (0.5-1mg) and surgically implanted. Kinetics and activities of released proteins were validated in ELISA analyses and in qPCR analyses of their target gene expression, respectively. Control Elvax40 polymer or Elvax40 polymers containing the above-mentioned proteins were implanted bilaterally into pubertal or adult *Gli2*$^{\Delta S}$ mice. Mammary ductal morphology was examined 7 days post-surgery. In parallel experiments, mammary ducts in the vicinity (1-2 mm) of implants were dissected and prepared as single cell suspensions. Cells derived from various implants were plated in 24-well peri-dish for 2 hours to deplete fibroblasts, followed by collection of supernatant enriched in epithelial cells. Total RNAs were extracted from epithelial cells and converted to cDNAs, which were then applied to gene-specific (Bio-Rad) pre-amplification and subsequent qPCR analyses.

GH, Estrogen and prolactin ELISA analyses in serum

Peripheral blood was drawn by retro-orbital bleeding in the amount of 200 ul from *Gli2*^{WT} and *Gli2*$^{\Delta S}$ mice. Mice were allowed to recover for 5 days until the next collection. Blood were kept at ambient temperature for 30 min, followed by centrifugation at 3,000 rpm for 10 min. Serum in the supernatant were used immediately for ELISA analyses, or if not, aliquoted and stored at -80°C until next use. Serum samples were diluted and subjected to standard ELISA assays to de-

termine GH or prolactin levels in accordance with manufacturer's protocol. Differences between genotypes are considered significant if $P<0.05$. Estrogen levels of *Gli2*^{WT} and *Gli2*$^{\Delta S}$ mice were determined by 17β-Estradiol ELISA kit (from Enzolifesciences) according to manufacturer's instructions.

Statistical analysis

Statistic analysis was performed using GraphPad Prism v5. Data are presented as mean±s.e.m., and group differences were examined with a two-tailed Student's *t*-test. P values were calculated based on three independent experiments unless otherwise specified. A value of $P<0.05$ is considered statistically significant.

Primers used in real-time RTPCR analysis

Primers used for pre-amplification of *Igf1*, *Egr1*, *mCsf*, *Axin2* in cDNAs of dissected implants were purchased from Bio-Rad. Primers used for qPCR analyses of *Col1a1*, *Col1a2*, *Col2a1*, *Pdgfrα*, *Pdgfβ*, and *Esr1* were previously reported (*50–52*). Others were purchased as QuantiTect Primer Assays from Qiagen. QuantiTect primer assays used for real-time rtPCR include *mGli2* (QT00291711), *Ghr* (QT00109900), *mBmp7* (QT00096026), *mIgf1* (QT00154469), *mWnt2* (QT00118503), *mWnt2b* (QT00115451), *mFgf7* (QT00172004), *mHgf* (QT00158046), *mEgr1* (QT00265846), *mCsf1* (QT01164324), *mIl-3Rα* (QT00251293), *mAxin2* (QT00126539) and *mLef1* (QT00148834).

REFERENCES AND NOTES

1. J. Briscoe, P. P. Thérond, The mechanisms of Hedgehog signalling and its roles in development and disease. *Nat. Rev. Mol. Cell Biol.* **14**, 416–429 (2013). doi:10.1038/nrm3598 Medline
2. K. Shin, J. Lee, N. Guo, J. Kim, A. Lim, L. Qu, I. U. Mysorekar, P. A. Beachy, Hedgehog/Wnt feedback supports regenerative proliferation of epithelial stem cells in bladder. *Nature* **472**, 110–114 (2011). doi:10.1038/nature09851 Medline
3. A. Lim, K. Shin, C. Zhao, S. Kawano, P. A. Beachy, Spatially restricted Hedgehog signalling regulates HGF-induced branching of the adult prostate. *Nat. Cell Biol.* **16**, 1135–1145 (2014). doi:10.1038/ncb3057 Medline
4. M. T. Lewis, S. Ross, P. A. Strickland, C. W. Sugnet, E. Jimenez, C. Hui, C. W. Daniel, The Gli2 transcription factor is required for normal mouse mammary gland development. *Dev. Biol.* **238**, 133–144 (2001). doi:10.1006/dbio.2001.0410 Medline
5. A. Pertzelan, L. Yalon, R. Kauli, Z. Laron, A comparative study of the effect of oestrogen substitution therapy on breast development in girls with hypo- and hypergonadotrophic hypogonadism. *Clin. Endocrinol. (Oxf)* **16**, 359–368 (1982). Medline
6. M. M. França, A. A. L. Jorge, L. R. S. Carvalho, E. F. Costalonga, G. A. Vasques, C. C. Leite, B. B. Mendonca, I. J. P. Arnhold, Novel heterozygous nonsense GLI2 mutations in patients with hypopituitarism and ectopic posterior pituitary lobe without holoprosencephaly. *J. Clin. Endocrinol. Metab.* **95**, E384–E391 (2010). doi:10.1210/jc.2010-1050 Medline
7. M. M. França, A. A. Jorge, L. R. Carvalho, E. F. Costalonga, A. P. Otto, F. A. Correa, B. B. Mendonca, I. J. Arnhold, Relatively high frequency of non-synonymous GLI2 variants in patients with congenital hypopituitarism without holoprosencephaly. *Clin. Endocrinol. (Oxf)* **78**, 551–557 (2013). Medline
8. E. Roessler, A. N. Ermilov, D. K. Grange, A. Wang, M. Grachtchouk, A. A. Dlugosz, M. Muenke, A previously unidentified amino-terminal domain regulates transcriptional activity of wild-type and disease-associated human GLI2. *Hum. Mol. Genet.* **14**, 2181–2188 (2005). doi:10.1093/hmg/ddi222 Medline
9. M. Y. Lee, L. Sun, J. M. Veltmaat, Hedgehog and Gli signaling in embryonic mammary gland development. *J. Mammary Gland Biol. Neoplasia* **18**, 133–138 (2013). doi:10.1007/s10911-013-9291-7 Medline
10. J. M. Veltmaat, F. Relaix, L. T. Le, K. Kratochwil, F. G. Sala, W. van Veelen, R. Rice, B. Spencer-Dene, A. A. Mailleux, D. P. Rice, J. P. Thiery, S. Bellusci, Gli3-mediated somitic Fgf10 expression gradients are required for the induction and patterning of mammary epithelium along the embryonic axes. *Development* **133**, 2325–2335 (2006). doi:10.1242/dev.02394 Medline
11. M. Y. Lee, V. Racine, P. Jagadpramana, L. Sun, W. Yu, T. Du, B. Spencer-Dene, N. Rubin, L. Le, D. Ndiaye, S. Bellusci, K. Kratochwil, J. M. Veltmaat, Ectodermal influx and cell hypertrophy provide early growth for all murine mammary rudiments, and are differentially regulated among them by Gli3. *PLOS ONE* **6**, e26242 (2011). doi:10.1371/journal.pone.0026242 Medline
12. S. J. Hatsell, P. Cowin, Gli3-mediated repression of Hedgehog targets is required for normal mammary development. *Development* **133**, 3661–3670 (2006). doi:10.1242/dev.02542 Medline
13. N. J. Kenney, G. H. Smith, E. Lawrence, J. C. Barrett, D. S. Salomon, Identification of stem cell units in the terminal end bud and duct of the mouse mammary gland. *J. Biomed. Biotechnol.* **1**, 133–143 (2001). doi:10.1155/S1110724301000304 Medline
14. L. Bai, L. R. Rohrschneider, s-SHIP promoter expression marks activated stem cells in developing mouse mammary tissue. *Genes Dev.* **24**, 1882–1892 (2010). doi:10.1101/gad.1932810 Medline
15. B. E. Welm, S. B. Tepera, T. Venezia, T. A. Graubert, J. M. Rosen, M. A. Goodell, Sca-1(pos) cells in the mouse mammary gland represent an enriched progenitor cell population. *Dev. Biol.* **245**, 42–56 (2002). doi:10.1006/dbio.2002.0625 Medline
16. G. H. Smith, D. Medina, Re-evaluation of mammary stem cell biology based on in vivo transplantation. *BCR* **10**, 203 (2008). doi:10.1186/bcr1856 Medline
17. J. E. Visvader, G. H. Smith, Murine mammary epithelial stem cells: Discovery, function, and current status. *Cold Spring Harb. Perspect. Biol.* **3**, a004879 (2011). doi:10.1101/cshperspect.a004879 Medline
18. J. E. Visvader, J. Stingl, Mammary stem cells and the differentiation hierarchy: Current status and perspectives. *Genes Dev.* **28**, 1143–1158 (2014). doi:10.1101/gad.242511.114 Medline
19. H. Moses, M. H. Barcellos-Hoff, TGF-beta biology in mammary development and breast cancer. *Cold Spring Harb. Perspect. Biol.* **3**, a003277 (2011). doi:10.1101/cshperspect.a003277 Medline
20. J. Mao, K. L. Ligon, E. Y. Rakhlin, S. P. Thayer, R. T. Bronson, D. Rowitch, A. P. McMahon, A novel somatic mouse model to survey tumorigenic potential applied to the Hedgehog pathway. *Cancer Res.* **66**, 10171–10178 (2006). doi:10.1158/0008-5472.CAN-06-0657 Medline
21. J. Taipale, J. K. Chen, M. K. Cooper, B. Wang, R. K. Mann, L. Milenkovic, M. P. Scott, P. A. Beachy, Effects of oncogenic mutations in Smoothened and Patched can be reversed by cyclopamine. *Nature* **406**, 1005–1009 (2000). doi:10.1038/35023008 Medline
22. M. Shackleton, F. Vaillant, K. J. Simpson, J. Stingl, G. K. Smyth, M.-L. Asselin-Labat, L. Wu, G. J. Lindeman, J. E. Visvader, Generation of a functional mammary gland from a single stem cell. *Nature* **439**, 84–88 (2006). doi:10.1038/nature04372 Medline
23. J. Stingl, P. Eirew, I. Ricketson, M. Shackleton, F. Vaillant, D. Choi, H. I. Li, C. J. Eaves, Purification and unique properties of mammary epithelial stem cells. *Nature* **439**, 993–997 (2006). Medline
24. C. Brisken, S. Duss, Stem cells and the stem cell niche in the breast: An integrated hormonal and developmental perspective. *Stem Cell Rev.* **3**, 147–156 (2007). doi:10.1007/s12015-007-0019-1 Medline
25. M. D. Sternlicht, Key stages in mammary gland development: The cues that regulate ductal branching morphogenesis. *BCR* **8**, 201 (2006). doi:10.1186/bcr1368 Medline
26. V. Gouon-Evans, M. E. Rothenberg, J. W. Pollard, Postnatal mammary gland development requires macrophages and eosinophils. *Development* **127**, 2269–2282 (2000). Medline
27. G. A. Wood, J. E. Fata, K. L. Watson, R. Khokha, Circulating hormones and estrous stage predict cellular and stromal remodeling in murine uterus. *Reproduction*

133, 1035–1044 (2007). doi:10.1530/REP-06-0302 Medline
28. N. M. Badders, S. Goel, R. J. Clark, K. S. Klos, S. Kim, A. Bafico, C. Lindvall, B. O. Williams, C. M. Alexander, The Wnt receptor, Lrp5, is expressed by mouse mammary stem cells and is required to maintain the basal lineage. *PLOS ONE* **4**, e6594 (2009). doi:10.1371/journal.pone.0006594 Medline
29. Y. A. Zeng, R. Nusse, Wnt proteins are self-renewal factors for mammary stem cells and promote their long-term expansion in culture. *Cell Stem Cell* **6**, 568–577 (2010). doi:10.1016/j.stem.2010.03.020 Medline
30. W. Ruan, D. L. Kleinberg, Insulin-like growth factor I is essential for terminal end bud formation and ductal morphogenesis during mammary development. *Endocrinology* **140**, 5075–5081 (1999). Medline
31. S. G. Bonnette, D. L. Hadsell, Targeted disruption of the IGF-I receptor gene decreases cellular proliferation in mammary terminal end buds. *Endocrinology* **142**, 4937–4945 (2001). doi:10.1210/endo.142.11.8500 Medline
32. M. L. Asselin-Labat, F. Vaillant, J. M. Sheridan, B. Pal, D. Wu, E. R. Simpson, H. Yasuda, G. K. Smyth, T. J. Martin, G. J. Lindeman, J. E. Visvader, Control of mammary stem cell function by steroid hormone signalling. *Nature* **465**, 798–802 (2010). doi:10.1038/nature09027 Medline
33. P. A. Joshi, H. W. Jackson, A. G. Beristain, M. A. Di Grappa, P. A. Mote, C. L. Clarke, J. Stingl, P. D. Waterhouse, R. Khokha, Progesterone induces adult mammary stem cell expansion. *Nature* **465**, 803–807 (2010). doi:10.1038/nature09091 Medline
34. M. L. Asselin-Labat, M. Shackleton, J. Stingl, F. Vaillant, N. C. Forrest, C. J. Eaves, J. E. Visvader, G. J. Lindeman, Steroid hormone receptor status of mouse mammary stem cells. *J. Natl. Cancer Inst.* **98**, 1011–1014 (2006). doi:10.1093/jnci/djj267 Medline
35. F. Darendeliler, A. Lindberg, P. Wilton, Response to growth hormone treatment in isolated growth hormone deficiency versus multiple pituitary hormone deficiency. *Horm. Res. Paediatr.* **76** (suppl. 1), 42–46 (2011). doi:10.1159/000329161 Medline
36. M. Maghnie, L. Ambrosini, M. Cappa, G. Pozzobon, L. Ghizzoni, M. G. Ubertini, N. di Iorgi, C. Tinelli, S. Pilia, G. Chiumello, R. Lorini, S. Loche, Adult height in patients with permanent growth hormone deficiency with and without multiple pituitary hormone deficiencies. *J. Clin. Endocrinol. Metab.* **91**, 2900–2905 (2006). doi:10.1210/jc.2006-0050 Medline
37. S. J. Morrison, D. T. Scadden, The bone marrow niche for haematopoietic stem cells. *Nature* **505**, 327–334 (2014). doi:10.1038/nature12984 Medline
38. C. B. Bai, A. L. Joyner, Gli1 can rescue the in vivo function of Gli2. *Development* **128**, 5161–5172 (2001). Medline
39. J. D. Corrales, S. Blaess, E. M. Mahoney, A. L. Joyner, The level of sonic hedgehog signaling regulates the complexity of cerebellar foliation. *Development* **133**, 1811–1821 (2006). doi:10.1242/dev.02351 Medline
40. M. D. Muzumdar, B. Tasic, K. Miyamichi, L. Li, L. Luo, A global double-fluorescent Cre reporter mouse. *Genesis* **45**, 593–605 (2007). doi:10.1002/dvg.20335 Medline
41. F. Strutz, H. Okada, C. W. Lo, T. Danoff, R. L. Carone, J. E. Tomaszewski, E. G. Neilson, Identification and characterization of a fibroblast marker: FSP1. *J. Cell Biol.* **130**, 393–405 (1995). doi:10.1083/jcb.130.2.393 Medline
42. G. Y. Lee, P. A. Kenny, E. H. Lee, M. J. Bissell, Three-dimensional culture models of normal and malignant breast epithelial cells. *Nat. Methods* **4**, 359–365 (2007). doi:10.1038/nmeth1015 Medline
43. J. L. Whyte, A. A. Smith, B. Liu, W. R. Manzano, N. D. Evans, G. R. Dhamdhere, M. Y. Fang, H. Y. Chang, A. E. Oro, J. A. Helms, Augmenting endogenous Wnt signaling improves skin wound healing. *PLOS ONE* **8**, e76883 (2013). doi:10.1371/journal.pone.0076883 Medline
44. C. R. Taylor, S.-R. Shi, C. Chen, L. Young, C. Yang, R. J. Cote, Comparative study of antigen retrieval heating methods: Microwave, microwave and pressure cooker, autoclave, and steamer. *Biotech. Histochem.* **71**, 263–270 (1996). doi:10.3109/10520299609117171 Medline
45. M. Diehn, R. W. Cho, N. A. Lobo, T. Kalisky, M. J. Dorie, A. N. Kulp, D. Qian, J. S. Lam, L. E. Ailles, M. Wong, B. Joshua, M. J. Kaplan, I. Wapnir, F. M. Dirbas, G. Somlo, C. Garberoglio, B. Paz, J. Shen, S. K. Lau, S. R. Quake, J. M. Brown, I. L. Weissman, M. F. Clarke, Association of reactive oxygen species levels and radioresistance in cancer stem cells. *Nature* **458**, 780–783 (2009). doi:10.1038/nature07733 Medline
46. P. Dalerba, T. Kalisky, D. Sahoo, P. S. Rajendran, M. E. Rothenberg, A. A. Leyrat, S. Sim, J. Okamoto, D. M. Johnston, D. Qian, M. Zabala, J. Bueno, N. F. Neff, J. Wang, A. A. Shelton, B. Visser, S. Hisamori, Y. Shimono, M. van de Wetering, H. Clevers, M. F. Clarke, S. R. Quake, Single-cell dissection of transcriptional heterogeneity in human colon tumors. *Nat. Biotechnol.* **29**, 1120–1127 (2011). doi:10.1038/nbt.2038 Medline
47. S. D. Robinson, G. B. Silberstein, A. B. Roberts, K. C. Flanders, C. W. Daniel, Regulated expression and growth inhibitory effects of transforming growth factor-beta isoforms in mouse mammary gland development. *Development* **113**, 867–878 (1991). Medline
48. W. Ruan, C. B. Newman, D. L. Kleinberg, Intact and amino-terminally shortened forms of insulin-like growth factor I induce mammary gland differentiation and development. *Proc. Natl. Acad. Sci. U.S.A.* **89**, 10872–10876 (1992). doi:10.1073/pnas.89.22.10872 Medline
49. W. Ruan, V. Catanese, R. Wieczorek, M. Feldman, D. L. Kleinberg, Estradiol enhances the stimulatory effect of insulin-like growth factor-I (IGF-I) on mammary development and growth hormone-induced IGF-I messenger ribonucleic acid. *Endocrinology* **136**, 1296–1302 (1995). Medline
50. M. J. Guerquin, B. Charvet, G. Nourissat, E. Havis, O. Ronsin, M.-A. Bonnin, M. Ruggiu, I. Olivera-Martinez, N. Robert, Y. Lu, K. E. Kadler, T. Baumberger, L. Doursounian, F. Berenbaum, D. Duprez, Transcription factor EGR1 directs tendon differentiation and promotes tendon repair. *J. Clin. Invest.* **123**, 3564–3576 (2013). doi:10.1172/JCI67521 Medline
51. E. D. Cohen, K. Ihida-Stansbury, M. M. Lu, R. A. Panettieri, P. L. Jones, E. E. Morrisey, Wnt signaling regulates smooth muscle precursor development in the mouse lung via a tenascin C/PDGFR pathway. *J. Clin. Invest.* **119**, 2538–2549 (2009). doi:10.1172/JCI38079 Medline
52. M. Kundakovic, K. Gudsnuk, B. Franks, J. Madrid, R. L. Miller, F. P. Perera, F. A. Champagne, Sex-specific epigenetic disruption and behavioral changes following low-dose in utero bisphenol A exposure. *Proc. Natl. Acad. Sci. U.S.A.* **110**, 9956–9961 (2013). doi:10.1073/pnas.1214056110 Medline

ACKNOWLEDGMENTS

This work was supported by a Susan G. Komen fellowship to C.Z., and funding from the U.S. Department of Defense, the Breast Cancer Research Foundation, and the Ludwig Institute for Cancer Research. The cell imaging core of Stanford Neuroscience Microscopy Service and the FACS core of Stanford Institute for Stem Cell Biology and Regenerative Medicine were supported by NIH core grants. We are grateful to K. M. Loh and J. Sage for critical reading and helpful discussion of this manuscript. P.A.B. is an investigator of the Howard Hughes Medical Institute.

SUPPLEMENTARY MATERIALS

www.sciencemag.org/cgi/content/full/science.aal3485/DC1
Figs. S1 to S10

5 November 2016; accepted 1 March 2017
Published online 9 March 2017
10.1126/science.aal3485

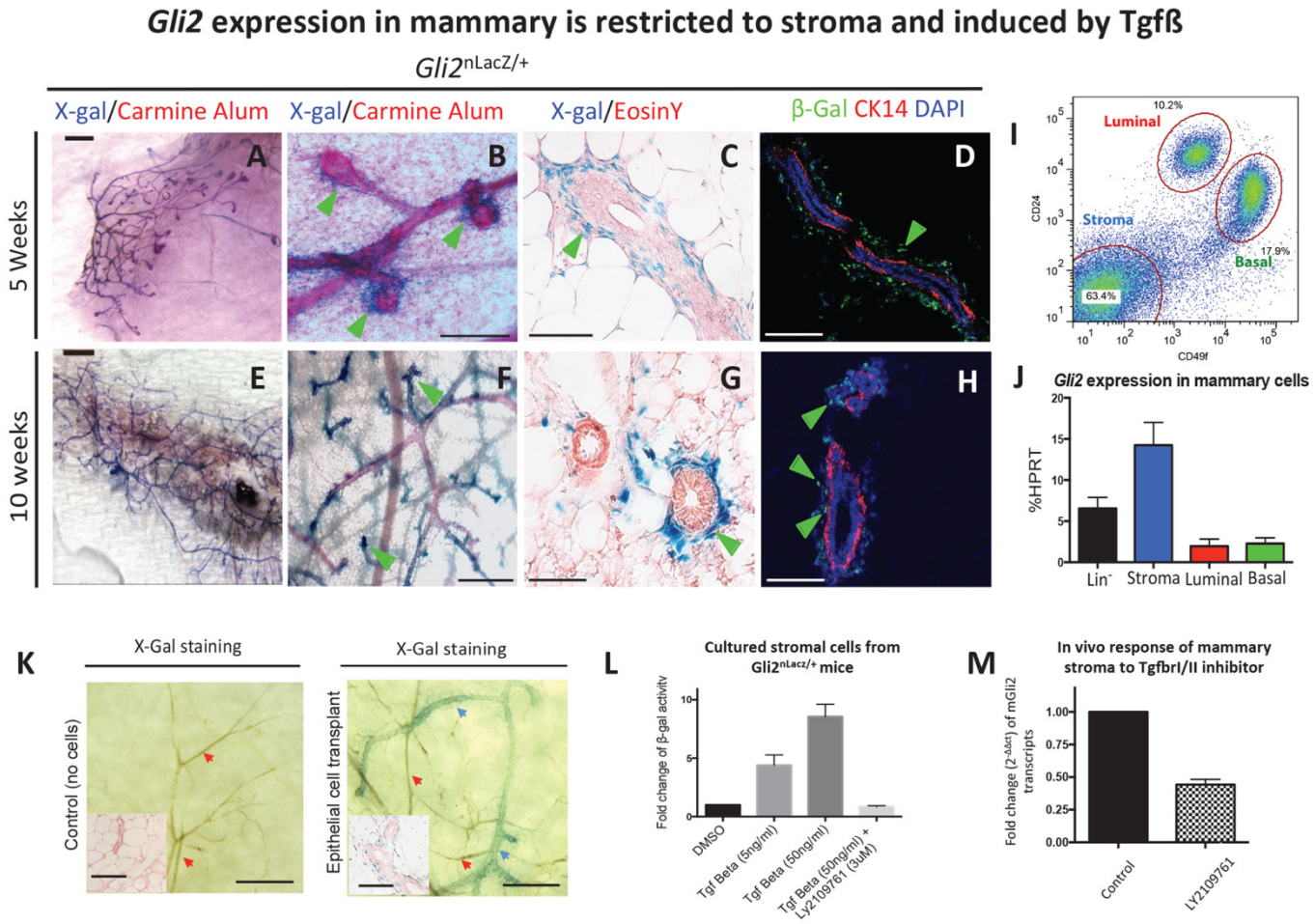

Fig. 1. ***Gli2*** **expression in mammary is restricted to stroma and induced by Tgfβ.** (**A**, **B**, **C**, **F**) Representative whole mount carmine alum stains and β-galactosidase activity stains (X-Gal) of the 4th mammary gland of Gli2$^{nLacZ/+}$ mice at 5-week-old pubertal (**A**, **B**) or 10-week-old adult (**E**, **F**) stages (n=6 for each stage). Note heavier X-gal staining at terminal structures (arrowheads). Scale bar, 500 μm. (**C**, **G**) X-gal/Eosin counter stain and (**D**, **H**) CK14/β-Gal immunofluorescence stain of cross sections showing stromal expression of *Gli2* (arrowheads). Scale bar, 50 μm. (**I**, **J**) Stromal cells, epithelial basal, and epithelial luminal cells from 10-week-old mice (n=5) were FACS-isolated and analyzed by qRT-PCR for *Gli2* mRNA expression bottom panel. *Gli2* levels were 6.55%, 14.24%, 1.97%, and 2.28% for total lineage$^-$ (Lin$^-$), stromal, luminal, and basal epithelial cells, respectively. (**K**) X-Gal staining showing epithelial cell-induced stromal Gli2 expression in mammary whole mount (scale bar, 1 mm) and in EosinY counter-stained mammary sections (inserts; scale bar, 50 μm). Red arrows point to the vasculature, and blue arrows point to the transplanted epithelial ducts. n=3 mice (6 transplants) per condition. (**L**) FACS-sorted mammary stromal cells derived from Gli2$^{nLacZ/+}$ mice were stimulated as indicated and representative changes of β-gal activity were measured and normalized to control samples. n=3 replicates per condition. (**M**) Gli2 qPCR analysis showing reduction of *Gli2* transcripts in FACS-isolated mammary stromal cells of mice treated with Tgfβ inhibitor, LY2109761, for 5 days as compared with vehicle treatment. (n=3 mice per treatment).

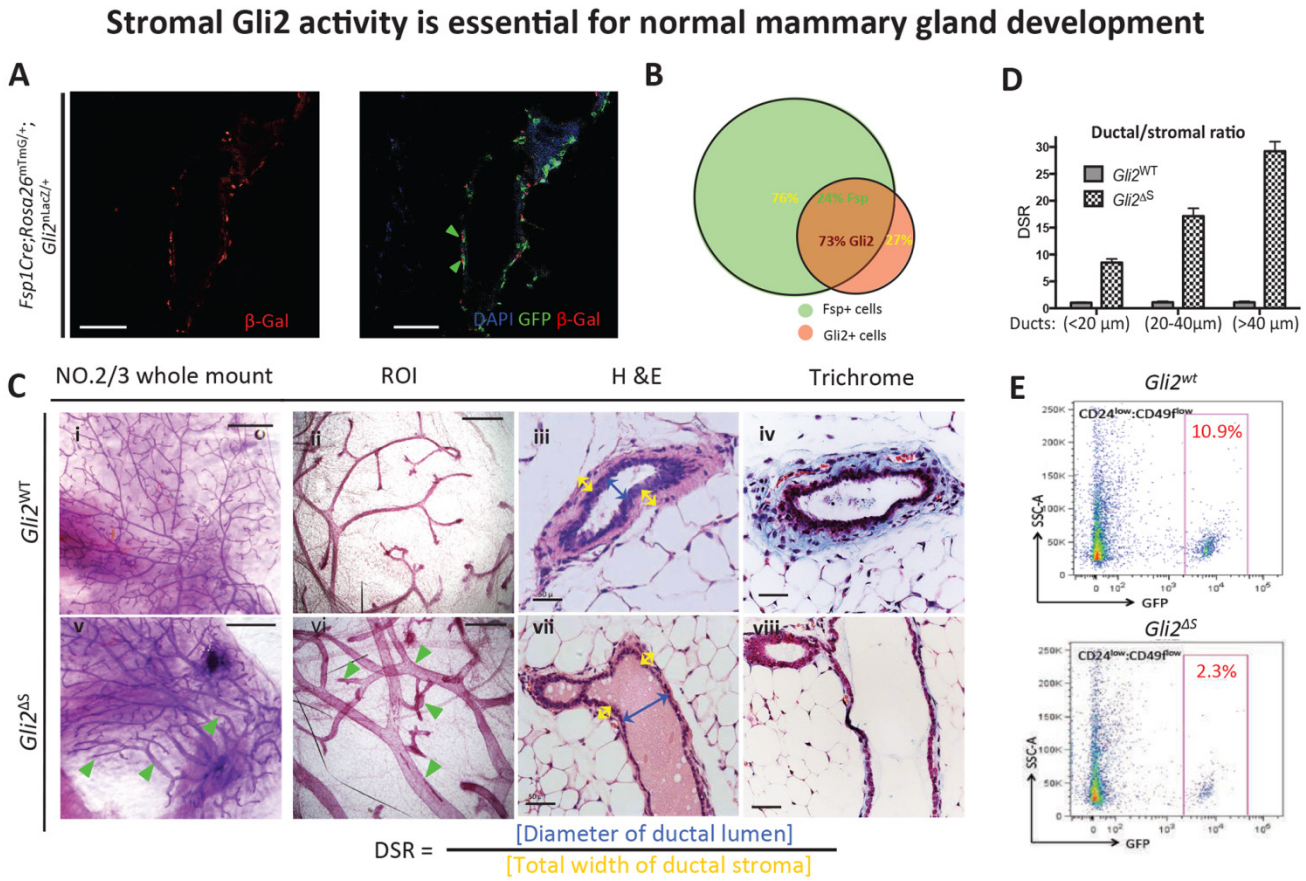

Fig. 2. Stromal *Gli2* activity is essential for normal mammary development. (**A**) Representative immunostaining showing coincident stromal cell expression of *Gli2*^{nLacZ} and *Fsp1*^{Cre} in mammary sections of *Fsp1*^{Cre};*Rosa26*$^{mTmG/+}$;*Gli2*$^{nLacZ/+}$ mice. *Gli2* expressing cells were pseudo-colored in red. Note that membrane-localized mGFP encircles nuclear-localized β-Gal. Scale bar, 50μm. (**B**) Venn diagram showing that *Fsp1*^{Cre}-expressing cells include the majority of *Gli2*-expressing cells as well as other stromal cells. (**C**) Representative whole mount carmine alum staining (i, iv), H&E staining (ii, v) and trichrome staining (iii, vi) of the 2nd&3rd mammary glands in 10-week-old *Gli2*^{WT} and *Gli2*^{ΔS} littermate mice. Note enlarged ducts and disrupted terminal structures in *Gli2*^{ΔS} (arrowheads in iv). The ductal to stromal ratio (DSR, panels ii, iv) is defined as the diameter of the ductal lumen (blue) divided by the total width of ductal stroma (yellow). Scale bars, 500 μm (i, iv) or 25 μm (ii, iii, v, vi). (**D**) DSR score, as defined in (**C**), for ducts of the indicated width classes in *Gli2*^{WT} vs *Gli2*^{ΔS} mice. Note that a significantly higher DSR of ducts in various width classes is associated with *Gli2*^{ΔS} mice. (10 ducts of indicated width within each class from the 2nd/3rd mammary glands of littermate mice were analyzed). (**E**) Representative analysis of FACS-isolated stromal cells from littermate *Gli2*^{WT} vs *Gli2*^{ΔS} mice (n=5) for expression of mGFP. Note the five-fold reduction of *Fsp1*-labeled stromal cells in the *Gli2*^{ΔS} mammary gland.

Stromal *Gli2* supports mammary epithelial stem cell regeneration

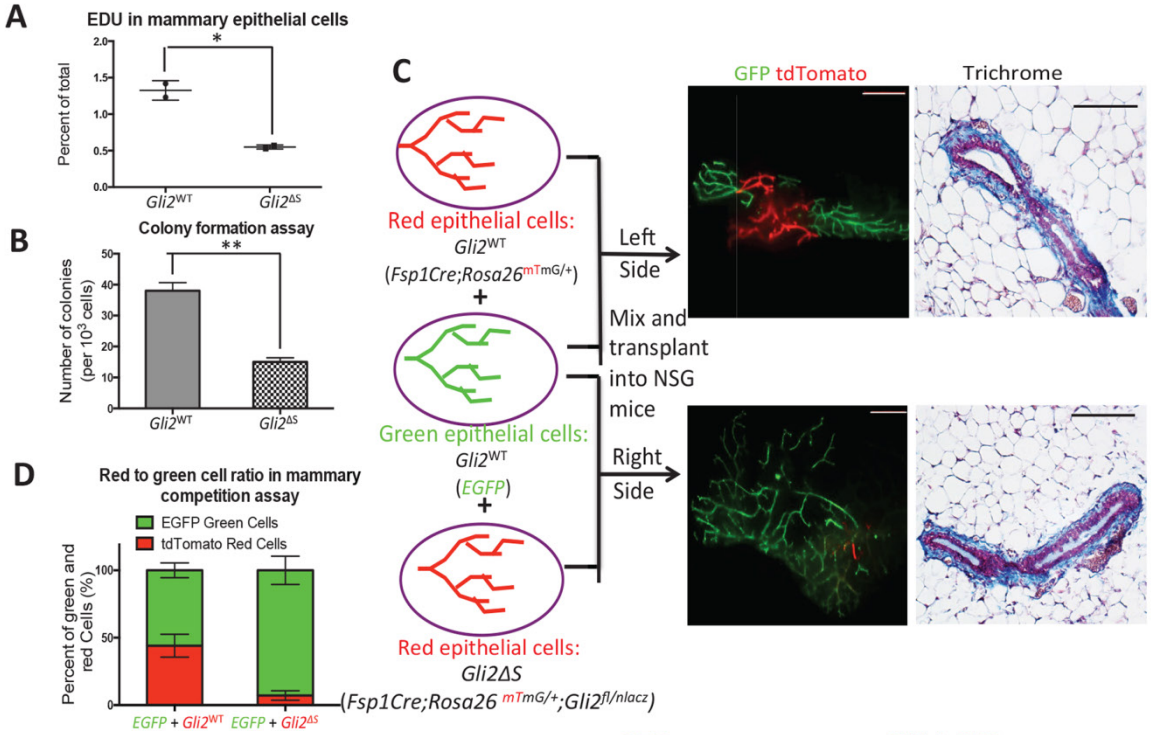

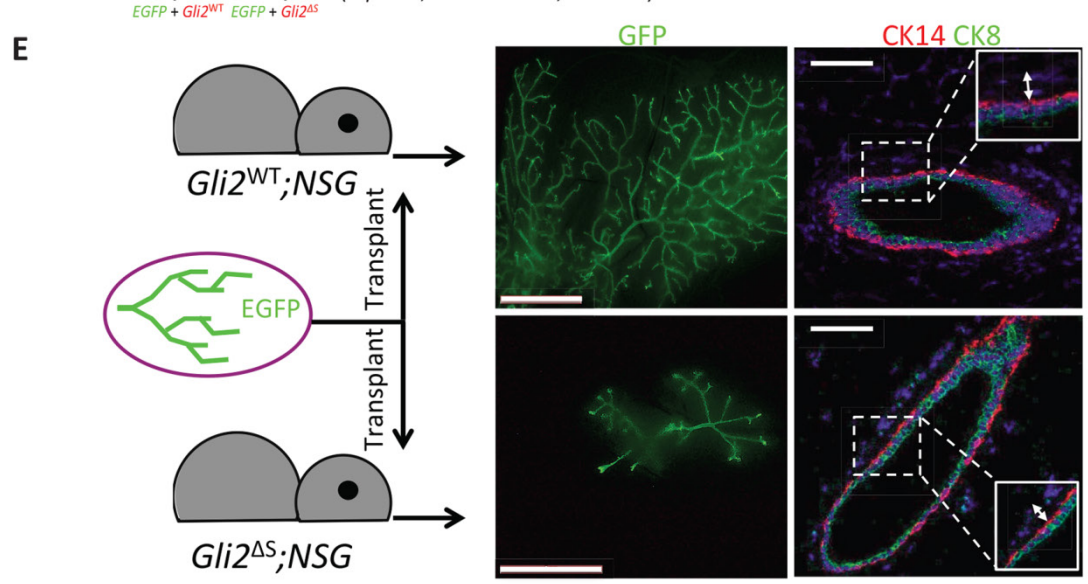

F

Donor: CAG-EGFP CD24+CD49fhigh:GFP+	Cells/ fat pad	Out-growths	Fat pad filled	Outgrowth efficiency (95% CI)
Recipient: *Gli2fl/+;NSG* or *Gli2nlacz/+;NSG*	50	3/8	X1 X2 X5	1 / 618 (375-1017)
	500	5/9	X2 X3 X4	
	1000	7/9	X4 X3 X2	
	2000	9/10	X6 X3 X1	
Recipient: *Fsp1cre;Gli2fl/nlacz;NSG* or *Fsp1cre;Gli2fl/fl;NSG*	50	0/6	X6	1 / 2920 (1436-5938)
	500	2/9	X2 X7	
	1000	3/8	X1 X2 X5	
	2000	3/8	X1 X2 X5	

Fig. 3. Stromal *Gli2* supports mammary epithelial stem cell regeneration. (**A**) Percent EDU$^+$ mammary epithelial cells as determined by FACS analysis 5 hours after EDU injection from *Gli2*^{WT} (*Gli2*$^{flox/+}$) and *Gli2*$^{\Delta S}$ (*Fsp1*^{Cre}*:Gli2*$^{nLacZ/flox}$) littermate mice (n=5 per genotype). (**B**) Colonies formed per 10^3 input epithelial cells within 10 days of culture in Matrigel were measured in triplicate from five individual *Gli2*^{WT} or *Gli2*$^{\Delta S}$ mice. (**C**, **D**) A Lin$^-$CD24$^+$CD49f^{hi}GFP$^+$ basal epithelial cell population enriched in MRU was FACS-isolated from EGFP mice and mixed with similarly isolated Lin$^-$CD24$^+$CD49f^{hi}tdTomato$^+$ basal epithelial cells from *Gli2*^{WT} or *Gli2*$^{\Delta S}$ mice for competitive repopulation assays. Cell mixtures transplanted into bilateral pairs of cleared fat pads were analyzed for outgrowth after 9 weeks. In the representative outgrowths shown, the red epithelial cells from *Gli2*^{WT} mice generate a higher proportion of the outgrowth (44 ± 8.5%) as compared to red epithelial cells derived from *Gli2*$^{\Delta S}$ mice (7 ± 3.5%). Scale bar, 2mm. No differences in stromal abundance were noted in trichrome staining of cross-sections of repopulated mammary glands. Scale bar, 50μm. 10 independent transplants into 5 NSG animals per condition were used to generate the bar graph in Fig. 2D. (**E**) Lin$^-$CD24$^+$CD49f^{hi}GFP$^+$ cells were FACS-isolated, serially diluted, and transplanted into cleared fat pads of immunocompromised (NSG) *Gli2*^{WT} or *Gli2*$^{\Delta S}$ mice. Outgrowths were analyzed by whole mount immunostaining, with representative images shown for outgrowths from the 2000 cell transplantations (**E**). Cross sections show no differences of CK14/CK8 expression in ducts grown in *NSG;Gli2*^{WT} or *NSG*;*Gli2*$^{\Delta S}$ hosts, although ducts in *NSG*;*Gli2*$^{\Delta S}$ hosts were distended. Scale bars, 5 mm (whole mount) and 50 μm (sections). (**F**) Results from transplantation of a range of cell numbers are shown as total outgrowths and as the proportion of these outgrowths that are greater than 20 mm^2 in size. Outgrowth efficiency is calculated based on total outgrowths by L-Calc™ software of StemCell Technologies. Data are presented as mean ± s.e.m., and significance was calculated by an unpaired Student's *t* test (*P<0.05%, **P<0.01).

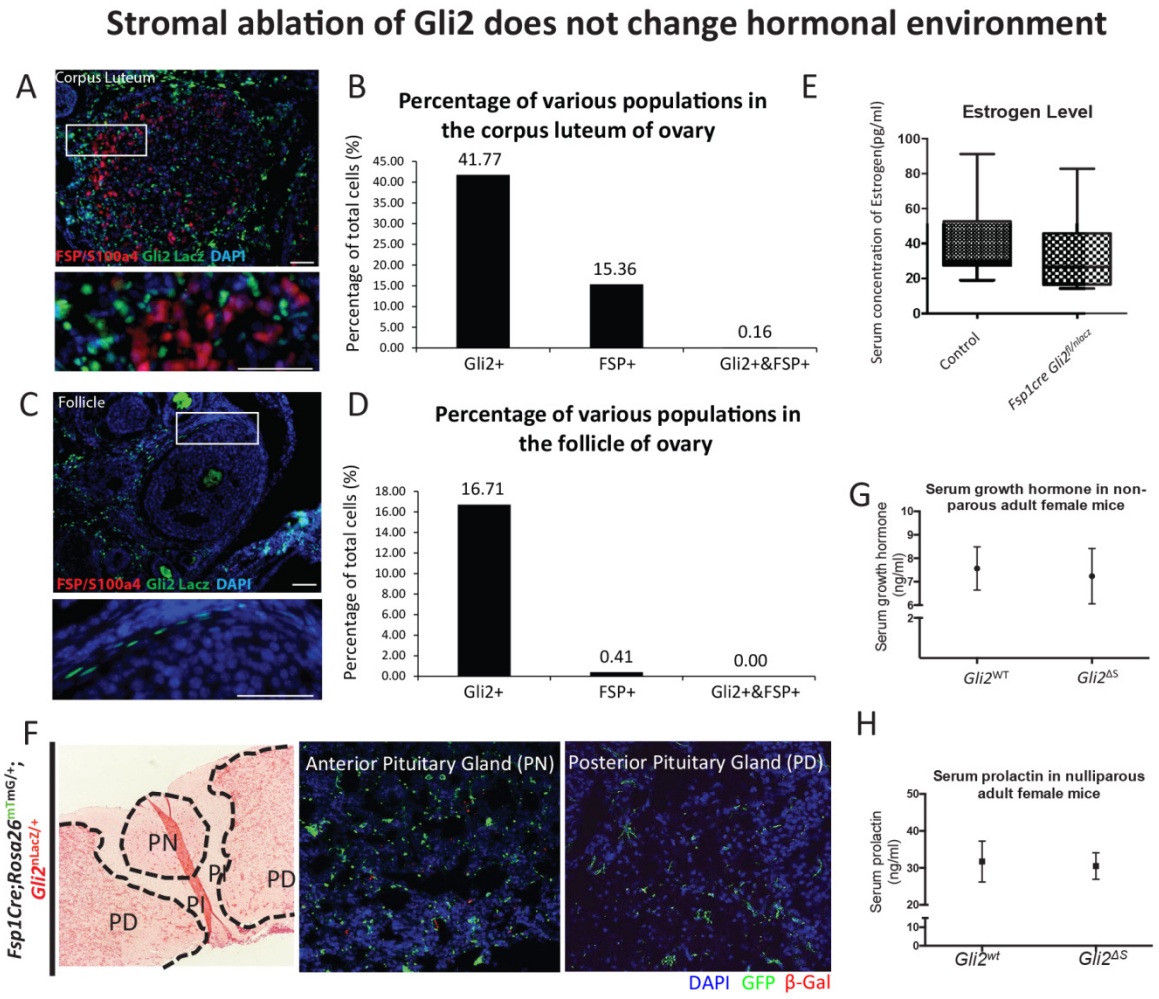

Fig. 4. Stromal *Gli2* ablation does not affect mammatrophic ovarian or pituitary hormones. (**A-D**) Staining for β-galactosidase and and FSP/S100a4 was performed in a *Gli2*$^{nLacZ/+}$ mouse ovary. β-galalactosidase (green), FSP/S100a4 (red) and nuclei (DAPI, blue) are shown in corpus luteum (**A**, **B**) and follicle (**C**, **D**). Quantitative analysis (**B**, **D**) involved counting more than 2000 cells. Scale bar, 100um. (**E**) Serum from *Gli2*^{WT} (n=12) and *Gli2*$^{\Delta S}$ (n=8) mice were collected and probed for estrogen level by ELISA. No significant difference was found between wt and *Gli2*$^{\Delta S}$ mutant groups. (p=0.5). (**F**) Representative H&E (left panel) immunostaining (middle and right panels) showing *Gli2*-expressing cells are distinct from *Fsp1*^{Cre}-labeled cells in the anterior lobe of pituitary gland in *Fsp1*^{Cre};*Rosa26*$^{mTmG/+}$;*Gli2*$^{nLacZ/+}$ mice. β-galactosidase- (*Gli2*) expressing cells were pseudo-colored in red. Note lack of *Gli2* expression in the posterior lobe of pituitary gland. (**G**, **H**) Quantification of growth hormone and prolactin levels in serum by ELISA in *Gli2*^{WT} or *Gli2*$^{\Delta S}$ mice.

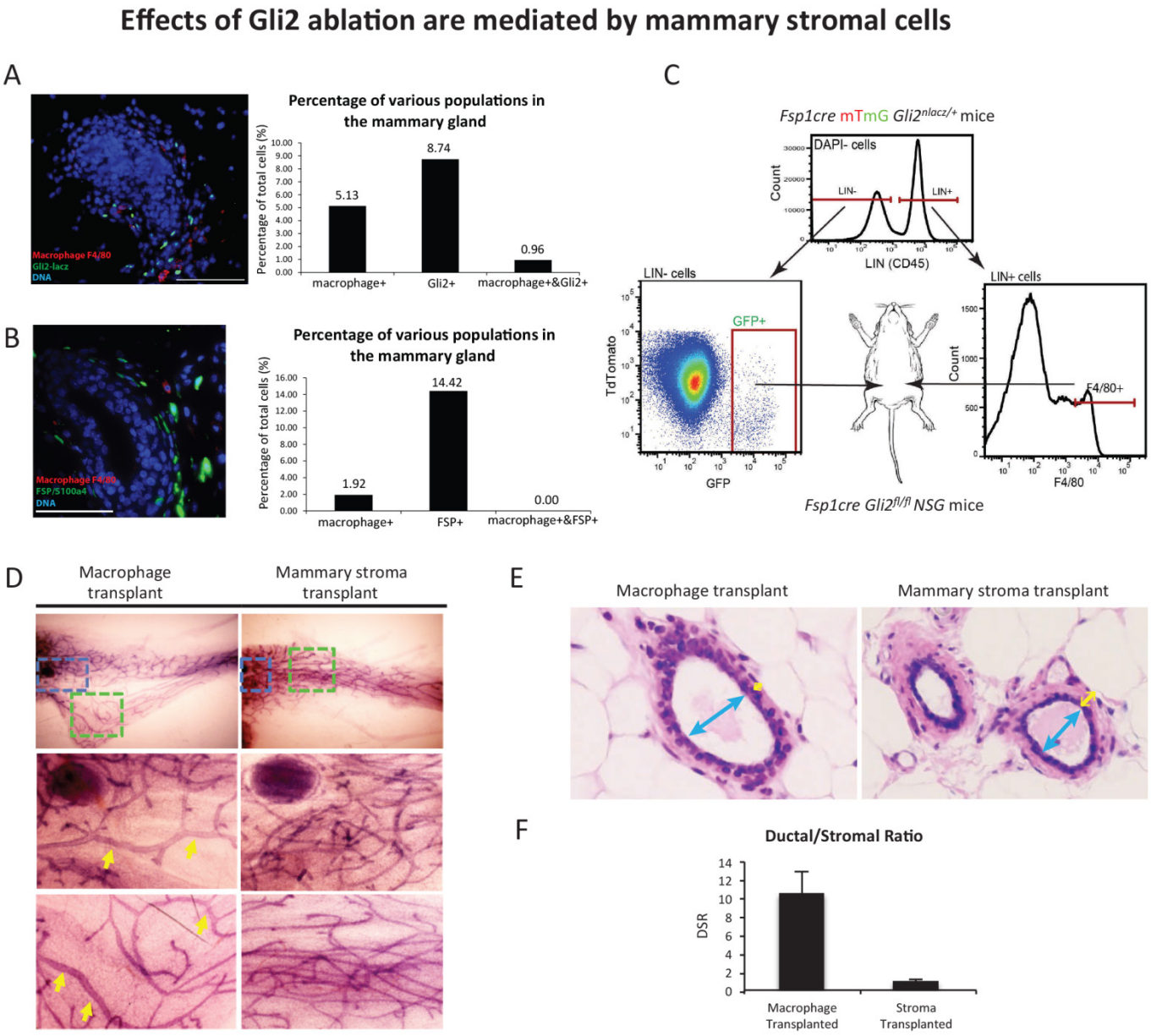

Fig. 5. Effects of *Gli2* ablation in *Gli2*$^{\Delta S}$ mice are mediated by mammary stromal cells. (**A**) Mammary gland from a 6 week old Gli2$^{LacZ/wt}$ mouse was paraffin sectioned and stained for LacZ for (Gli2 expression) and F4/80 (macrophage marker). Sections containing terminal end buds (TEBs) were analyzed and quantified for Gli2 (green) and macrophage (red) costaining. Scale bar, 100um. (**B**) Mammary gland from a 6 week old wt mouse was paraffin sectioned and stained for Fsp/S100a4 and the macrophage marker F4/80. Sections containing TEBs were analyzed and quantified for Fsp/S100a4 (green) and macrophage (red) co-staining. Scale bar, 100um. (**C**) *Fsp1*-expressing stromal cells and macrophages were sorted from an *Fsp1*^{Cre};*mTmG*;*Gli2*$^{nLacZ/+}$ mouse mammary gland and injected into the fat pads of *Fsp1*^{Cre};*Gli2*$^{fl/fl}$;NSG recipient mice. Two months after injection recipient mice were euthanized for whole mount analysis. (**D**) Fsp-expressing stromal cells rescue mammary duct enlargement whereas macrophages do not. N=3. (**E**, **F**) Mammary glands from *Gli2*$^{\Delta S}$;NSG recipients with injected donor macrophages/stroma were collected and sectioned for H&E staining, and DSR (ratio of ductal diameter, blue arrow, to total stromal width, yellow arrow) was determined as in Fig. 2. $p<0.01$.

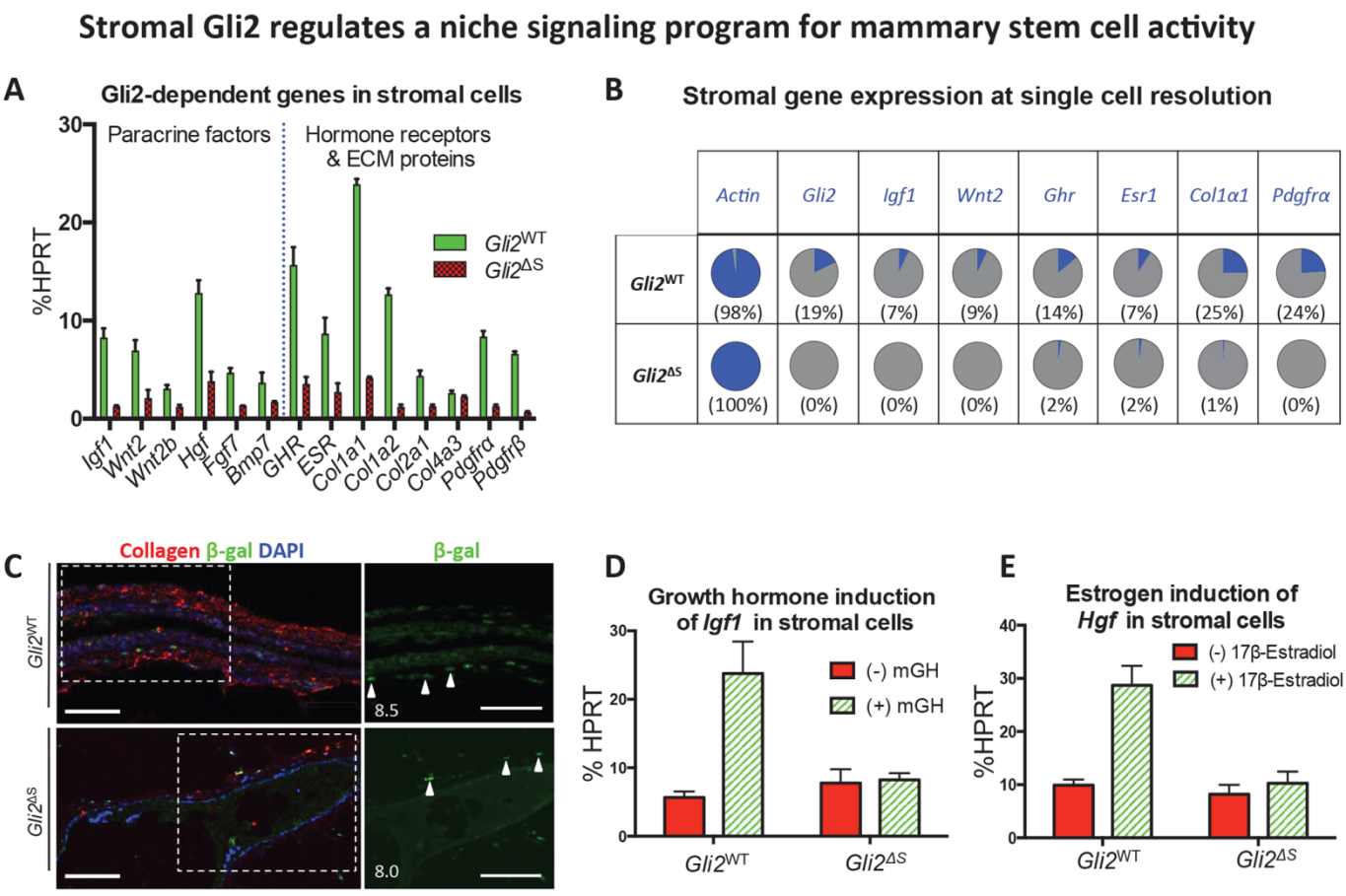

Fig. 6. Stromal *Gli2* regulates a niche signaling program for mammary stem cell activity. (**A**) *Fsp1*^{Cre}-labeled mammary stromal cells FACS-isolated from *Gli2*^{WT} (*Fsp1*^{Cre};*Rosa26*$^{mTmG/+}$) or *Gli2*$^{\Delta S}$ (*Fsp1*^{Cre};*Rosa26*$^{mTmG/+}$;*Gli2*$^{flox/nLacZ}$) littermate mice were analyzed by qRT-PCR for expression of selected genes, shown as a percentage of *HPRT* expression, and measured in triplicate from each of three individual *Gli2*^{WT} or *Gli2*$^{\Delta S}$ mice. Three major classes of stromally expressed genes are down-regulated in stromal cells of *Gli2*$^{\Delta S}$ mice (see text). (**B**) Gene expression in single, FACS-isolated *Fsp1*^{Cre}-labeled stromal cells from *Gli2*^{WT} and *Gli2*$^{\Delta S}$ mice was analyzed by qRT-PCR. The results (fig. S4) are summarized here as the percentage of single cells analyzed that express the indicated genes. (**C**) Sections of *Gli2*^{WT} (*Fsp1*^{Cre};*Rosa26*$^{mTmG/+}$;*Gli2*$^{nLacZ/+}$) and *Gli2*$^{\Delta S}$ (*Fsp1*^{Cre};*Rosa26*$^{mTmG/+}$;*Gli2*$^{nLacZ/flox}$) mammary glands immuno-stained for collagen and β-galactosidase. Selected areas (dotted lines) are shown at higher magnification in the green channel only (β-galactosidase-expressing cells) in the right panels. The frequency of β-galactosidase-labeled cells per 100 μm length of ductal epithelium is shown in the lower left of the right panels. Scale bar, 50 μm. (**D**, **E**) *Fsp1*^{Cre}-labeled mammary stromal cells FACS-isolated and cultured from *Gli2*^{WT} or *Gli2*$^{\Delta S}$ mice were stimulated with murine growth hormone (mGH) (**D**) or 17β-Estradiol (**E**) for 24 hours and assayed for expression of *Igf1* or *Hgf*, respectively. Note reduced expression of *Igf1* and *Hgf* in *Gli2*$^{\Delta S}$ as compared to *Gli2*^{WT}. Measurements in panels (**D**, **E**) were made in triplicate from each of three individual *Gli2*^{WT} or *Gli2*$^{\Delta S}$ mice.

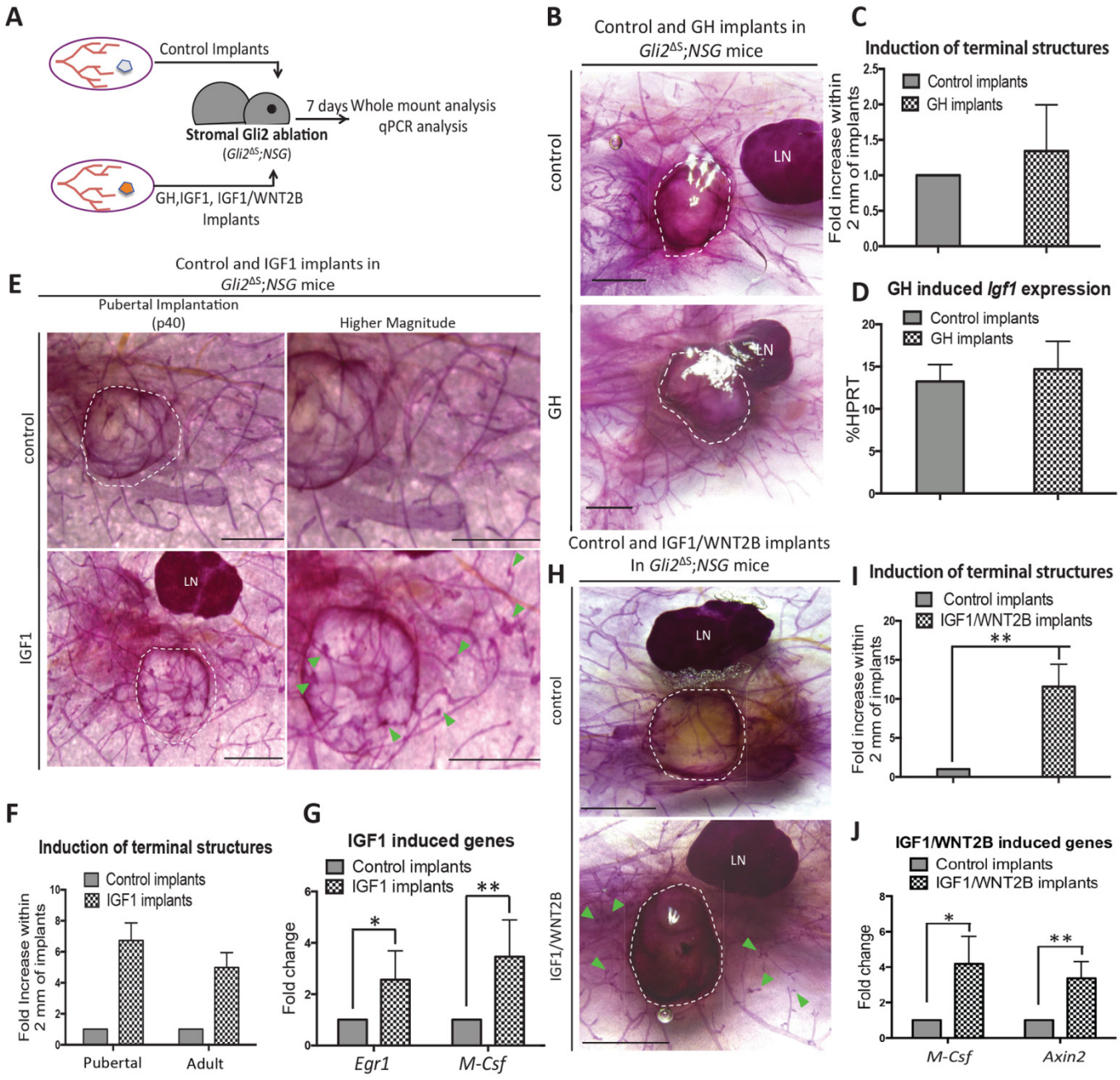

Fig. 7. Slow-release Igf1, Wnt2b polymer implants rescue epithelial growth defects in *Gli2*$^{\Delta S}$ mice. (**A**) Schematic of slow-release polymer-based implantation experiments to test activity of Gh, Igf1 and combined Igf1/Wnt2b. (**B**) Control and Gh-containing polymers (dashed lines) were implanted bilaterally into immuno-deficient *Gli2*$^{\Delta S}$ (*NSG: Gli2*$^{\Delta S}$) mice and ductal morphology was examined 7 days after implantation (n=3 implantations; one representative image of three is shown). Scale bar, 1 mm. (**C**) Numbers of terminal structures within 2 mm of implantation site are shown as fold increase relative to control implants. (**D**) Induction of Igf1 induction in control and GH-containing implants. Note that GH failed to induce terminal growth or *Igf1* expression in *NSG;Gli2*$^{\Delta S}$ mice. (**E**) Control and Igf1-containing polymers (dashed lines) were implanted bilaterally into *NSG;Gli2*$^{\Delta S}$ mice at pubertal (p40) or adult (p70) stages. Ductal morphology was examined after 7 days (n=3 implantations; one representative image of three is shown). Scale bar, 1 mm. (**F**, **G**) Numbers of terminal structures (**F**) within 2 mm of implants and Igf1-induced expression of *Egr1* and *M-Csf* (**G**) was calculated and normalized to control implants. (**H**) Control and Igf1/Wnt2b-containing polymers (dashed lines) were implanted bilaterally into *NSG;Gli2*$^{\Delta S}$ mice, followed by morphological analyses after 7 days (n=3 implantations; one representative image of three is shown). Scale bar, 1mm. (**I**, **J**) Numbers of terminal (**I**) structures and induction of IGF1 or WNT2b target genes (**J**) were quantified as fold increase relative to control implants. Note that IGF1/WNT2b implants induce more terminal end growth as compared to IGF1 alone. Data are normalized to the mean values in the control, and are presented as mean ± s.e.m.; statistical significance was calculated by an unpaired Student's *t* test (*P<0.05%, **P<0.01, ***P<0.001).

Mammary stem cell niche dysfunction in *Gli2*$^{\Delta S}$ mice and CPHD patients results from stromal loss of *Gli2*

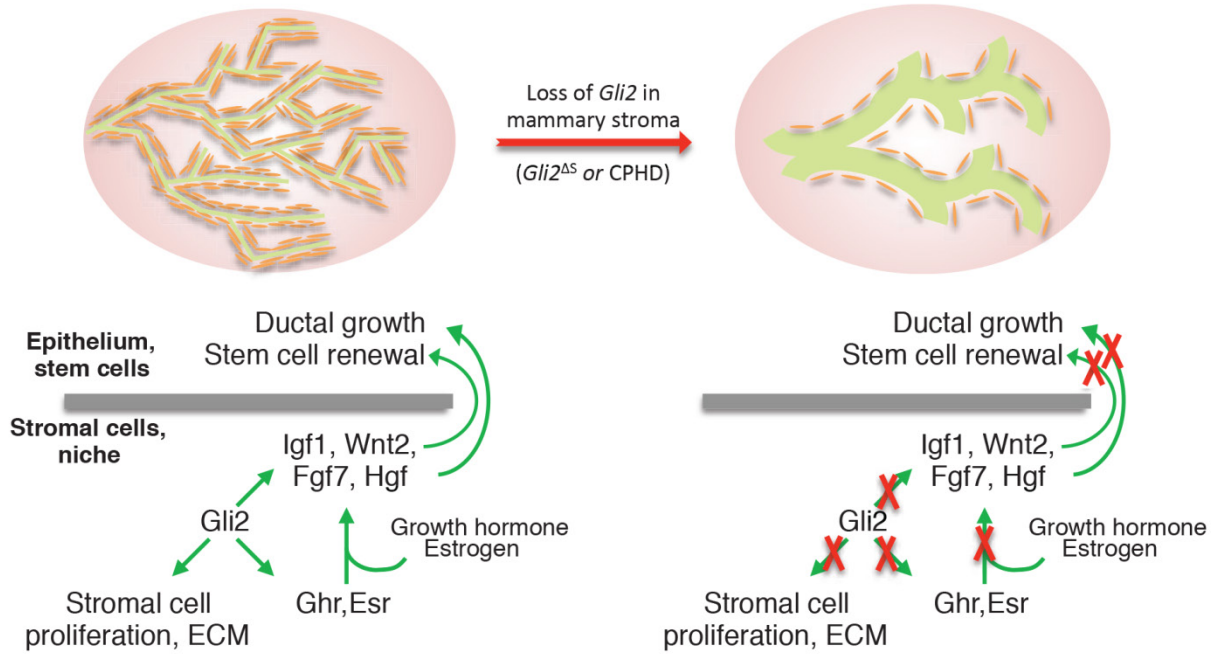

Fig. 8. Mammary stem cell niche dysfunction in *Gli2*$^{\Delta S}$ mice and CPHD patients results from stromal loss of *Gli2*. Normal *Gli2* function in mammary stroma (left) coordinates mammary stem cell niche signaling, response to estrogen and growth hormone, and stromal expansion, leading to normal mammary stem cell maintenance and hormone induced growth and morphogenesis at puberty. Stromal loss of *Gli2* function in *Gli2*$^{\Delta S}$ mice or CPHD (right) leads to disruption of the niche signaling program and loss of mammatrophic hormone response at puberty.

Stromal *Gli2* activity coordinates a niche signaling program for mammary epithelial stem cells

Chen Zhao, Shang Cai, Kunyoo Shin, Agnes Lim, Tomer Kalisky, Wan-Jin Lu, Michael F. Clarke and Philip A. Beachy (March 9, 2017)
published online March 9, 2017

Editor's Summary

Science (print ISSN 0036-8075; online ISSN 1095-9203) is published weekly, except the last week in December, by the American Association for the Advancement of Science, 1200 New York Avenue NW, Washington, DC 20005.